# SECTION 3. THE RADIATION ENVIRONMENT

## 3.1. THE EARTH'S MAGNETIC FIELD

### 3.1.1. The magnetosphere

The morphology, or spatial distribution, of the radiation environment experienced by Earth-orbiting spacecraft is largely a manifestation of the interaction of charged particles with the Earth's magnetic field. To a first approximation, this field is that of a magnetic dipole and, in those regions where the field lines are "closed", charged particles become trapped in the magnetosphere (see Section 3.2).

The field is not geographically symmetrical, however. Local distortions are caused by an offset and tilt of the magnetic axis with respect to the Earth's axis and by geological influences; one particularly marked feature is known as the "South Atlantic anomaly". This is important for low earth orbits. At high altitude, the effect of the solar wind is to distort the magnetosphere to a great degree. The resulting form of the field has characteristics comparable to the bow-wave and wake of a solid object moving through a fluid. This effect is well illustrated in Figure 3.1. The magnetosphere here is divided into regions of different trapping capability. The direction of the Sun is to the left of the figure.

The field is also not constant with time. Apart from short-term variations associated with storms, the strength of the field is decreasing with time at the rate of about 0.1% per year. The dipole moment, associated with the dipolar elements of the field currently has a value 0.304 gauss $(R_E)^3$, where $R_E$ is the Earth's radius.

### 3.1.2. Co-ordinates

It is useful to consider the magnetosphere and its associated radiation structure as a simplified structure. An idealised form of the Earth's field is used to define a system of co-ordinates by means of which points in the magnetosphere may be defined. Each field line (the surface of revolution of which is a "magnetic shell" or "drift shell") is defined by a parameter L (Mc Ilwain, 1961).

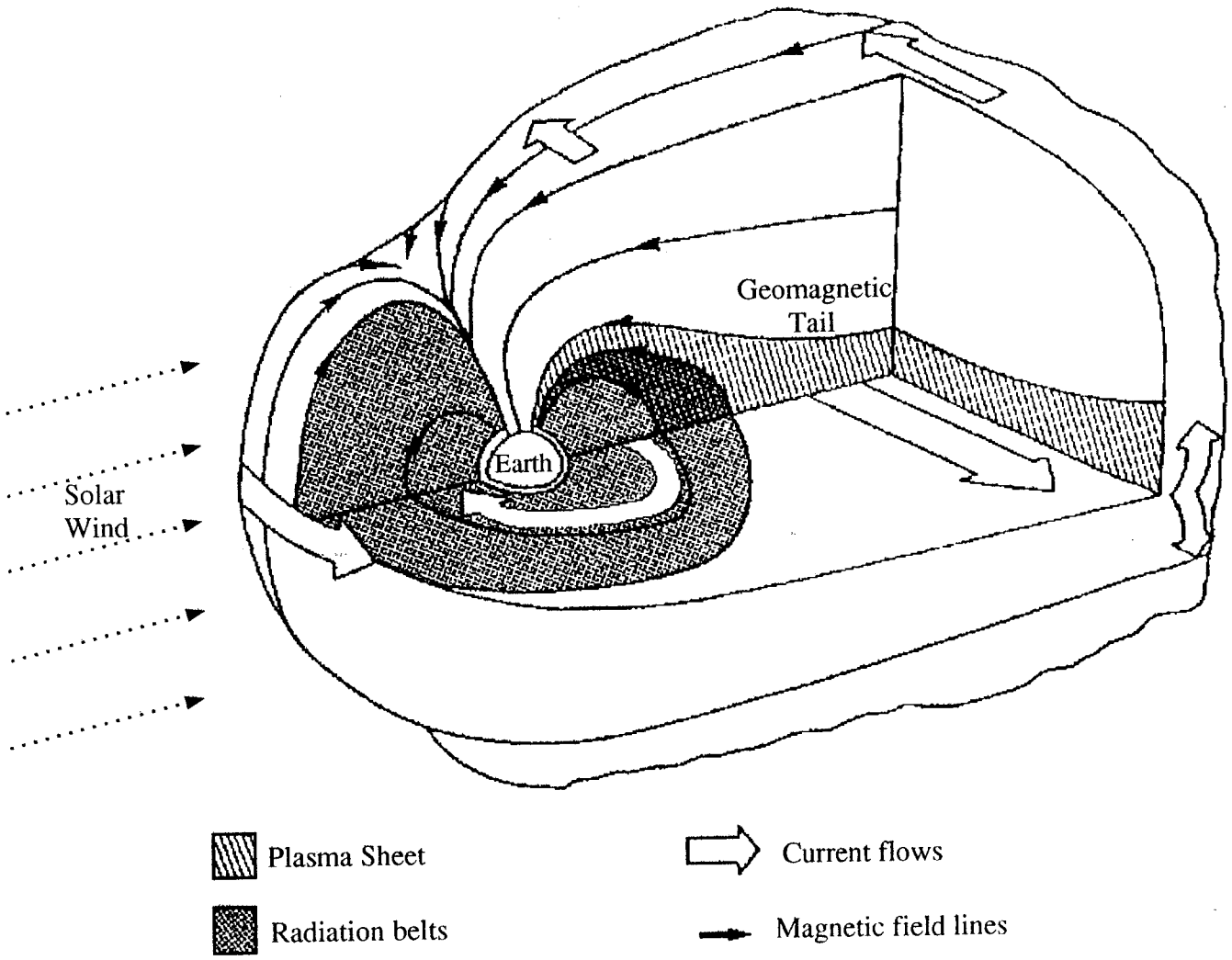


The Magnetosphere and Radiation Belts showing the distortion of the Earth's field which is approximately dipolar at low altitude and becomes strongly affected by the solar wind at high altitude. The Sun is to the left.

*FIGURE 3.1 - THE MAGNETOSPHERE AND RADIATION BELTS*

In an ideal dipole, this is equal to the geocentric radius at which the shell cuts the magnetic equator; it is measured in units of earth radii $R_E$ and all points on that field line and drift shell have the same L value. The position of a point on a field line is defined by a parameter B which is the magnetic field strength. At constant L, the value of B varies from a minimum at the magnetic equator to a maximum where the field line cuts the Earth's surface: B-L space is a fixed ideal co-ordinate system and is not affected by the temporal and local variations in the magnetosphere referred to earlier.

As an alternative, points may be defined in R-$\lambda$ space. This system does not refer to field lines or shells; R is the geocentric distance of the point and $\lambda$ is the magnetic latitude. Either co-ordinate system may be used in the appropriate circumstances. In this section, reference will be frequently made to the parameter L.

Mc Ilwain (1961) described a method whereby locations in the Earth's true internally generated field could be transformed numerically into the B-L. co-ordinates of an "equivalent perfect dipole".

Numerous computer-based models of the Earth's internally generated magnetic field are available, including the International Geophysical Reference Field, IGRF, which describe the field's spatial and long-term temporal variations. The National Space Science Data Centre, NSSDC, at NASA-GSFC provides these and other field models, including some which model the external source field corrections to the internal source. For radiation environment computations, an internal source field model is normally used.

## 3.2. TRAPPED RADIATION

The trapping of charged particles, in particular electrons and protons, by the Earth's magnetic field, creates the toroidal radiation belts known as the "Van Allen" belts which encircle the Earth (see Figure 3.1.)

A trapped charged particle follows a path spiralling about a line of force; it has an angular motion about the field line and a linear motion along it. The linear velocity is greatest at the magnetic equator where the field is weakest. As it moves along a line towards the poles and into regions of higher field strength, the linear component is reduced until a "mirror point" is reached where the particle is reflected back towards the equator, unless it is lost to the upper atmosphere. If it survives, the particle continually retraces its path back and forth along a field line while also drifting around the Earth (Hess, 1968).

This state of affairs is not entirely static. Particles are continually being lost to the atmosphere or are gained from extraterrestrial

origins, from the solar wind or cosmic-ray-induced neutron decay (Schultz, 1982). Schultz (1982) also indicates that Jupiter may be supplying significant fluxes of energetic electrons to the Earth's outer magnetosphere. The environment varies over a number of time scales. An important variation is that linked to the solar activity cycle. This cycle with a duration of approximately 11 years reflects the changing frequency of sunspots and solar flares and changes in the steady efflux of charged particles and electromagnetic radiation from the Sun. The rate of injection of particles into the Earth's trapped radiation environment and the Earth's atmospheric density both change over the solar cycle, influencing creation and loss processes and causing changes in the equilibrium fluxes.

In the past, the equilibrium was affected artificially by the injection of particles resulting from the explosion of nuclear devices. The American "Starfish" explosion in 1962 caused very large changes in trapped electron distribution, an effect which was unexpectedly stable and persisted until at least 1965. Military spacecraft are designed to survive such intentional injections of energetic "fission-spectrum" electrons.

Since the morphology of the belts is governed by the distorted dipole field, the belts are subject to the same spatial and time-dependent distortions. As with the magnetic field itself, it is often convenient to consider the structure of the belts in a time-averaged form. This is reasonable when the total radiation exposure of most spacecraft will be accumulated over a large number of orbits and a large number of days. Problems arise when the mission duration is short or when the short-term variations influence operations; for example, the variation of particle fluxes on the orbit of an astronomy mission which leads to detector background.

Figures 3.2 and 3.3 illustrate the average structure of the trapped electron and proton belts. The contours join points of equal average particle flux and are derived from the AE8 and AP8 environment models corresponding to solar-minimum conditions. In fact these figures are plotted as if the Earth's field were dipolar.

The electron environment consists of particles of energies up to about 7 MeV, with the most energetic particles occurring in the "outer zone" described below. In contrast, proton energies of several hundred MeV are found, the most energetic protons being found at lower altitudes.

It will be observed that the electron environment is so structured that there are two flux maxima; it is conventional to refer to the inner and outer electron zones, each zone being associated with one of the flux maxima. It will also be seen that the outer zone envelops the inner zone, its contours extending towards the Earth in cusps of relatively high flux. These extensions of the outer zone approach the Earth at high magnetic latitudes (60°-70°), the regions

associated with auroral phenomena. A line passing through these earthward extensions of successive flux contours is a field line cutting the magnetic equator at a geocentric distance of approximately 4.5 earth radii. The parameter L = 4.5 may therefore be taken as the "centre" of the outer zone. Similarly, the field line passing through the less obvious cusps of the inner zone is close to L = 1.4, while the "boundary" between the zones is marked by the field line close to L = 2.3.

The region between the zones is often referred to as the "slot", possibly a consequence of the combination of radial diffusion and losses induced by wave particle interactions (Lyons and Williams, 1984). The increase in trapped electron population at times of high solar activity results in a pronounced "slot-filling" tendency. The same effect was observed after artificial increases in electron population following nuclear tests. The structure of the trapped proton environment is simpler. There is a single belt with a flux maximum in the region of L = 1.7; this is also commonly referred to as the inner zone.

The effect of the South Atlantic Anomaly, where, because of the offset and tilt of the geomagnetic field, field lines containing significant energetic-particle fluxes approach the Earth's surface, is shown in Figure 3.4. The resulting flux enhancement close to South America on low orbits is apparent. Also clearly shown are the high-latitude enhancements where the geomagnetic field brings energetic, trapped, outer-zone electrons to low altitudes.

For practical purposes, the particle fluxes are normally regarded as isotropic. This is a simplification, as fluxes do in fact show important "anisotropies" in some places.

At low altitudes, in the South Atlanctic Anomaly, particle velocities are almost completely perpendicular to the field lines. In addition, atmospheric absorption of the gyrating particles results in a higher flux of protons from the west. For energetic protons at low altitudes, the ratio of fluxes can exceed two orders of magnitude.

The outer-zone electron environment is very dynamic, exhibiting large variations over a number of time scales. A 27-day periodicity in relativistic electron fluxes indicates a close link with solar wind streams and possibly Jupiter (Baker et al, 1986).

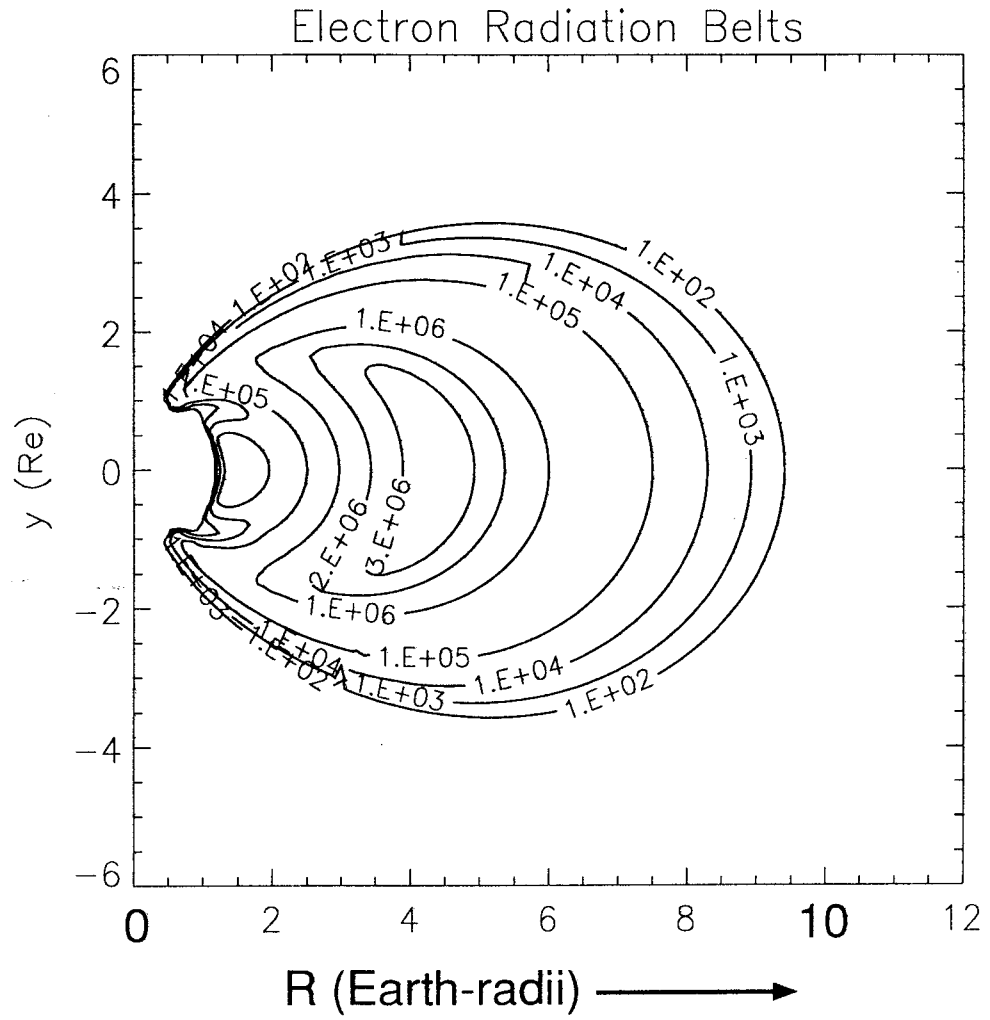


Radiation-belt electron model flux contours in "idealised dipole space". *z* is aligned with the dipole axis and *x* is a radial distance from the axis. Both are in units of earth radii.

*FIGURE 3.2 - TRAPPED ELECTRON RADIATION BELTS*

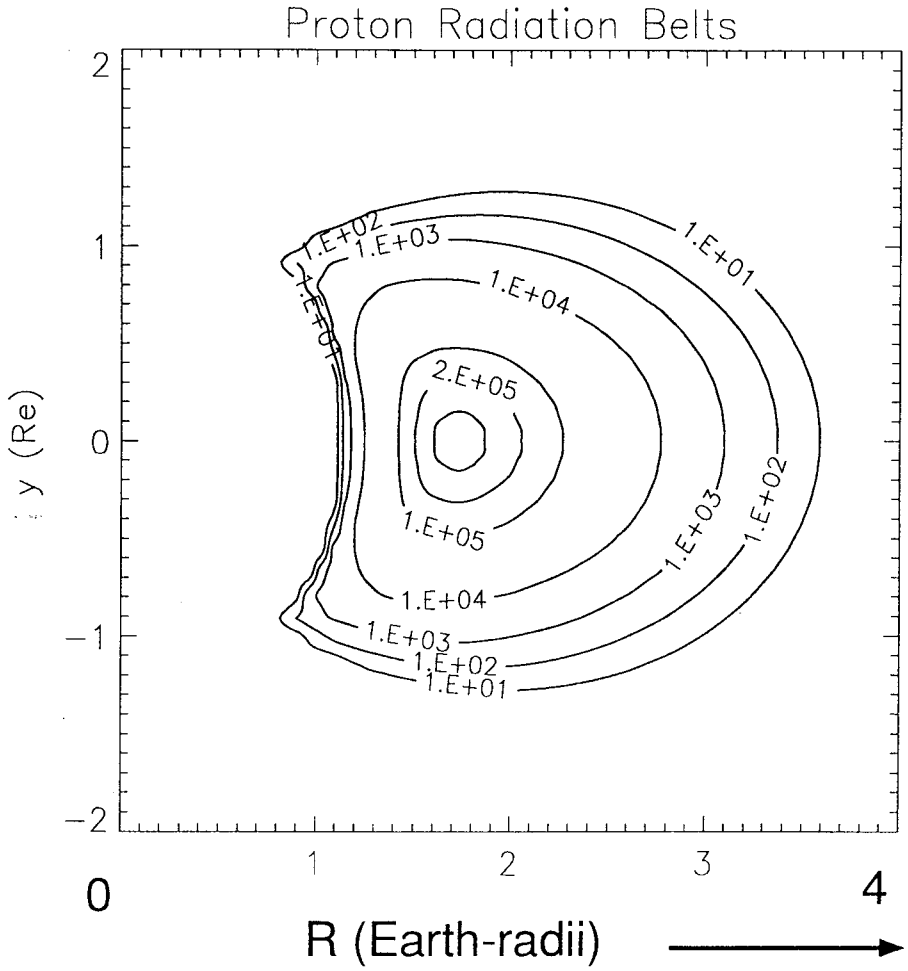


Radiation-belt proton model flux contours in "idealised dipole space".

*FIGURE 3.3 - TRAPPED PROTON RADIATION BELTS*

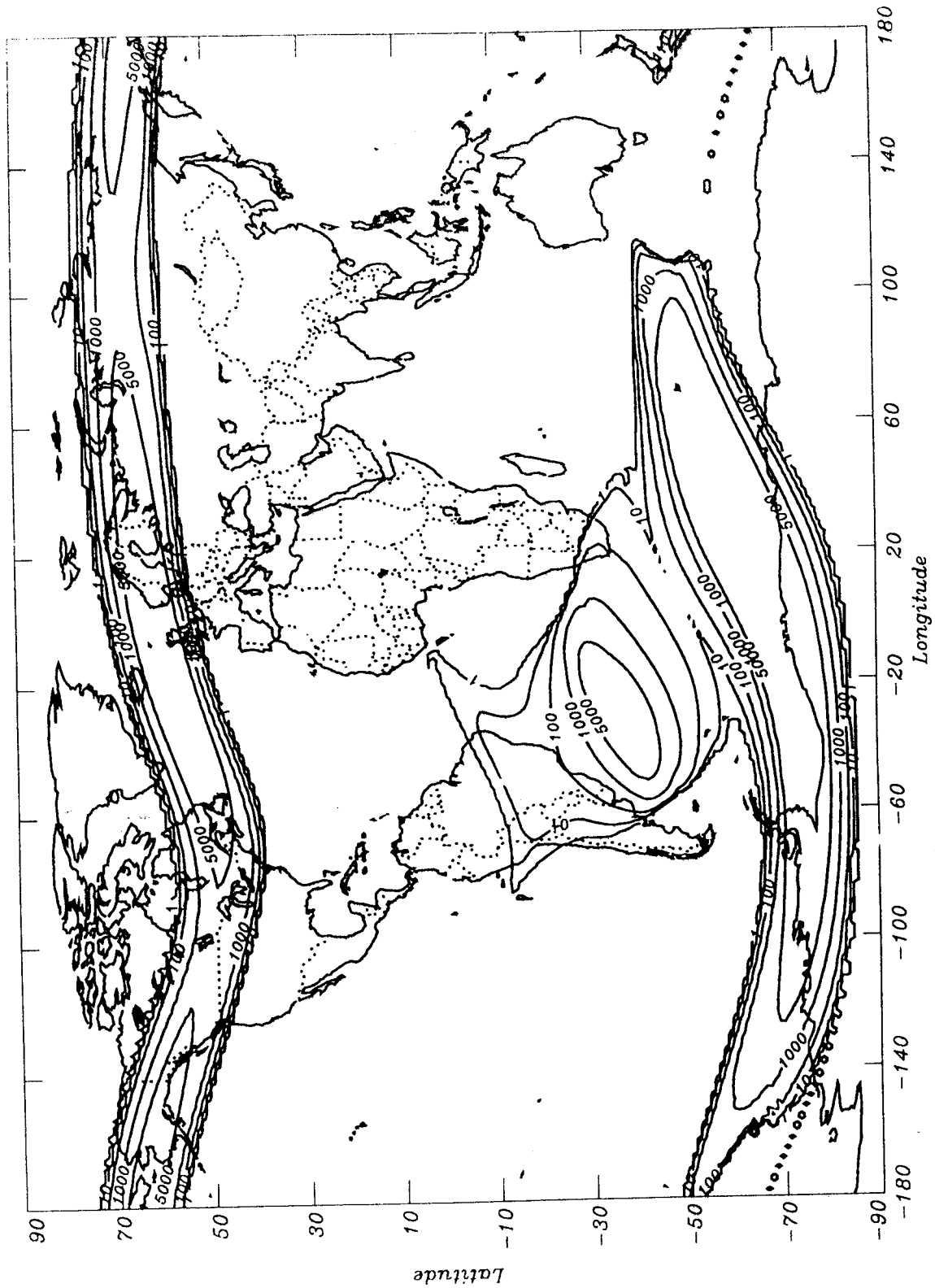


Contours of electron fluxes at > 1MeV showing the way in which the radiation belts, following the Earth's magnetic field come to low altitudes over the South Atlantic and at high latitudes

*FIGURE 3.4 - THE SOUTH ATLANTIC ANOMALY AND OUTER ZONE FLUXES*

## 3.3. SOLAR FLARES

In addition to exposure to the trapped radiation environment, a spacecraft is likely to encounter other transient radiation fluxes. The major effect to be considered is that due to solar flare protons. These particles, together with others such as electrons and alpha particles of a less significant nature, are emitted by the Sun in bursts during solar-flare activity ("solar storms") and their fluxes, besides being intermittent, vary overall with the solar cycle. The flux-energy spectra of solar protons are likely to be softer than those associated with trapped protons, but a spacecraft may nevertheless be exposed to considerable total fluence (time-integrated flux) levels. A single flare in August 1972 completely dominated the solar cycle number 20 (1964-1974) in terms of fluence and total dose. No flare as large was seen in cycle 21 (1974-1985), but Figure 3.5 (McGuire, 1983) shows that cycle 19 probably had a number of severe flares. The cycle in progress at the time of writing, cycle 22, contains a number of significant events. In particular, the October 1989 event was larger at low energies than that of August 1972 although it was still well below that event at E>10 MeV. Flare fluxes are about as predictable as most storms and are usually dealt with on a probability basis.

The degree of exposure to such effects is highly dependent upon orbital parameters. The Earth's magnetic field exhibits a shielding effect in equatorial regions, but allows the proton flux to be funnelled in towards the magnetic poles. (These protons produce the well-known polar absorption phenomenon in the ionosphere which has a strong disturbing effect on radio communications.) Thus, equatorial orbits will be shielded from solar-proton flux except at very high altitudes, whereas polar or highly inclined orbits may be greatly exposed even at low altitudes.

Geomatic shielding exhibits a significant east-west asymmetry, protons being able to penetrate to lower altitudes from the west than from the east. Disturbances in the magnetosphere also affect geomagnetic shielding. The shielding has been seen to weaken significantly in the wake of geomagnetic storms (Adams et al, 1981 and Daly, 1988).

## 3.4. COSMIC RAYS

### 3.4.1. Galactic cosmic rays

These are primary cosmic rays which originate outside the solar system but are associated with the galaxy. Cosmic rays are isotropic, highly energetic, charged particles, typically of 1 MeV to 1 GeV, although measurements have been made up to the 1 TeV range. They consist of electrons, protons and highly charged nuclei.

The most numerous particles are protons, with smaller populations of alpha particles, helium nuclei and decreasing numbers of the lighter nuclei. Beyond Z=30, the numbers of particles are very small. In addition, some Z>90 particles have been detected, but these are extremely rare.

Elemental abundances of galactic cosmic rays are shown in Figure 3.6 together with solar-system elemental abundances. For comparison, Figure 3.7 shows how the cosmic-ray abundances have been modified by fragmentation from their original source composition.

Variation of the overall galactic cosmic-ray flux is due to several effects. The most important effect is the intensity decrease during the solar maxima which occur in cycles of about 11 years (Figure 3.8). This flux decrease is thought to be due to the interaction of the galactic cosmic rays with the solar wind and so depends on the level of solar activity. Adams et al. (1981) chose a sine function as a means of predicting the modulation of their environment model:

$$M = A \sin \omega (t - t_o) + B \qquad \text{.....3(i)}$$

where: $\omega = 2\pi/10.9$ years$^{-1}$ = 0.576 radians/year, $t_o$ = 1950.6 and A and B are constants chosen for the best fit to the data.

### 3.4.2. Solar cosmic rays

In addition to producing an intense burst of UV and X-rays, solar flares accelerate solar material to high velocities. Solar-flare protons were discussed earlier, but particles of higher Z are also produced in abundance. These solar particles are similar to galactic cosmic rays but, owing to their different origin, are not identical in composition (Chenette and Dietrich, 1984). During a flare, cosmic rays are dominated at low and medium energies by solar material of low atomic weight. In addition, the extragalactic overall cosmic radiation in an earth orbit may increase dramatically. This is because solar flares cause geomagnetic disturbances resulting in considerable lowering of the geomagnetic barrier. The

importance of "geomagnetic shielding" will be discussed later. See Adams et al (1981) for a fuller discussion.

### 3.4.3. Terrestrial cosmic rays

The primary cosmic radiation which penetrates the Earth's atmosphere is rapidly transformed by interactions which produce a cascade of secondary radiation. These cascades take place in the main body of the atmosphere and the secondary rays produced are the principal component of cosmic radiation at the Earth's surface. This process has been described at length by Rossi (1964) and also by Ziegler (1979) in relation to electronic devices on the earth's surface. Tsao et al (1984) have recently studied the atmospheric cosmic-ray environment at high altitude.

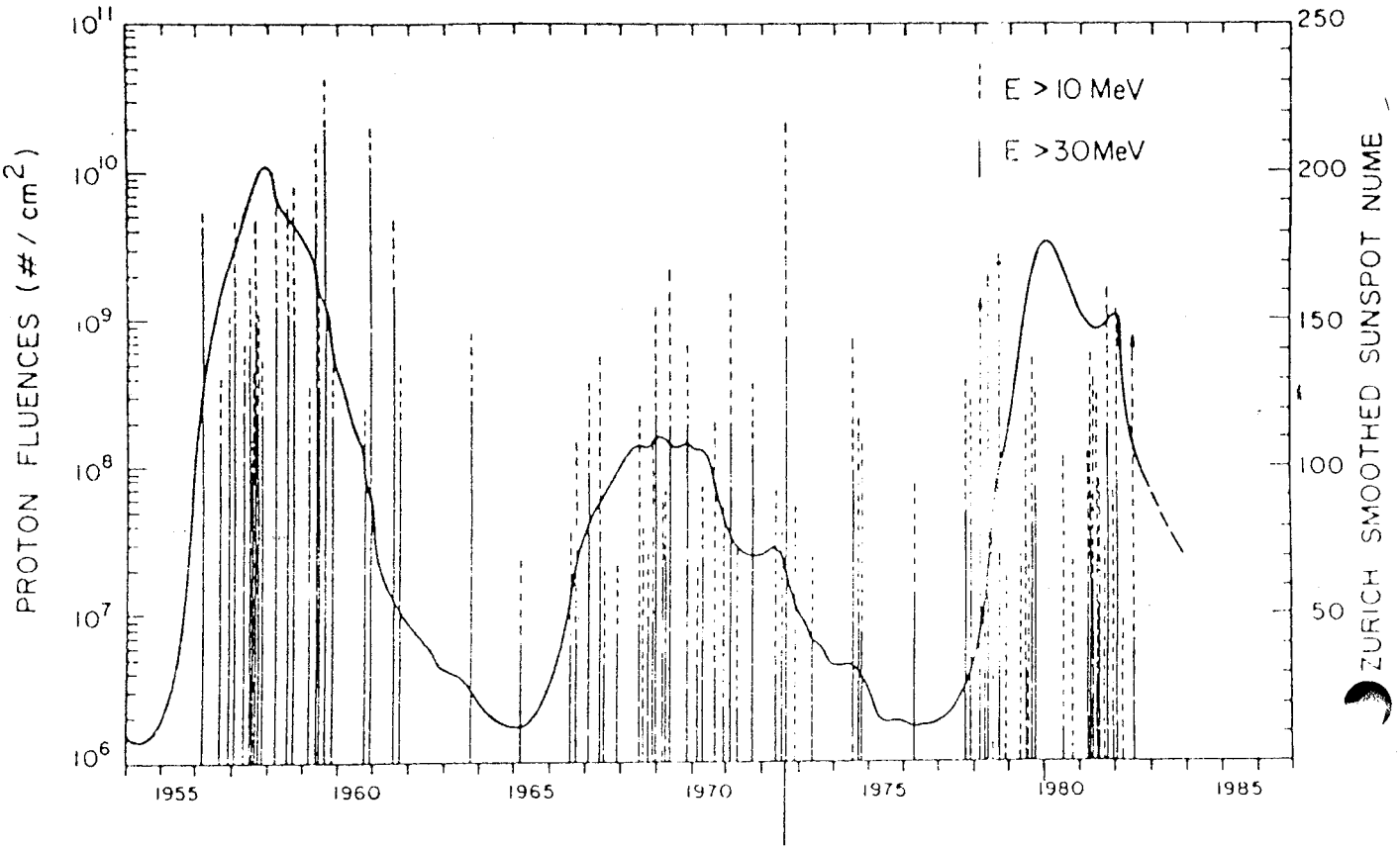


The occurrence of large solar-flare fluences (vertical lines) over the last three solar cycles superimposed on the sunspot number curve. The anomalous size of the August 1972 event is apparent.

*FIGURE 3.5 - SOLAR FLARES*

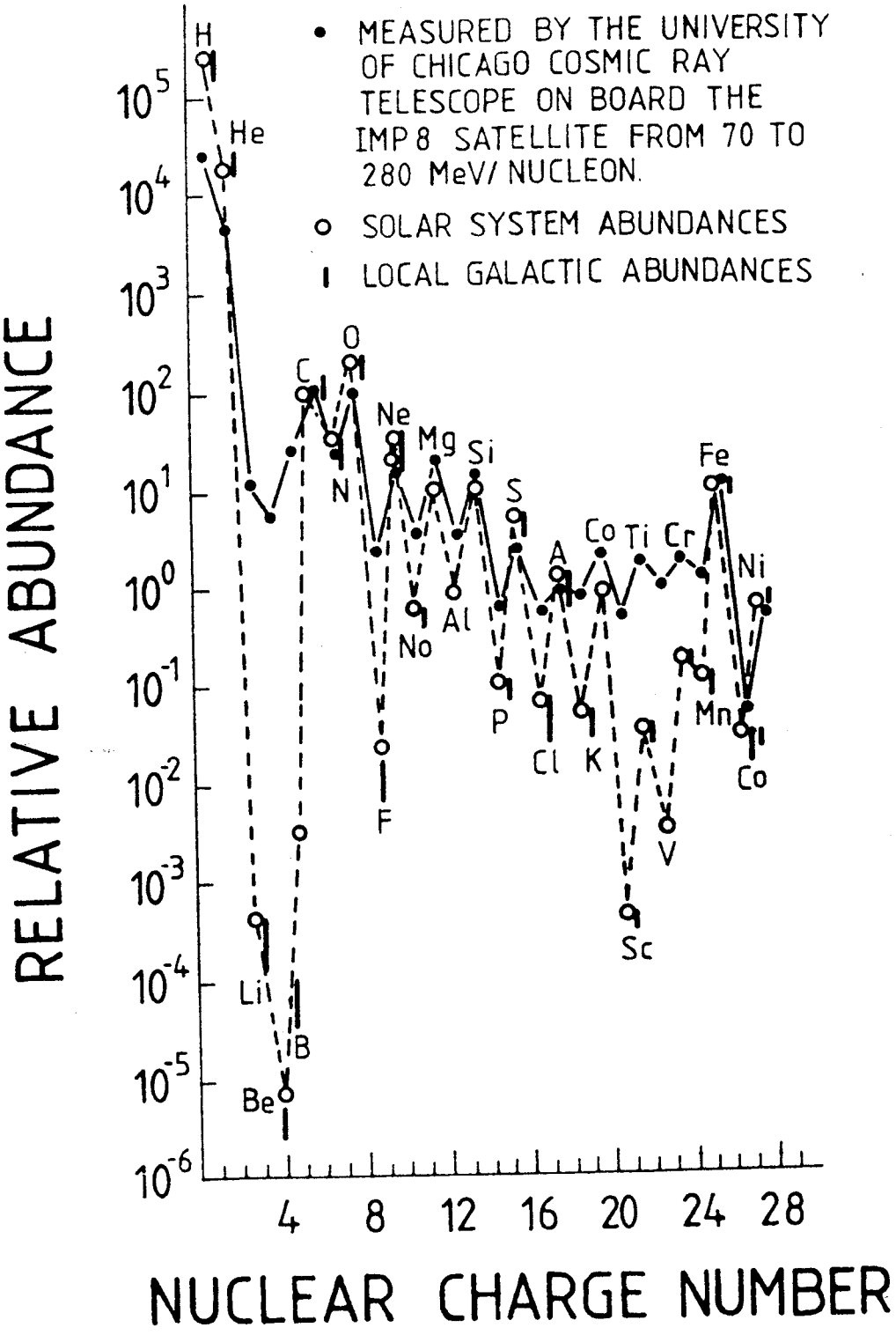


*FIGURE 3.6 - ELEMENTAL ABUNDANCE OF GALACTIC COSMIC RAYS COMPARED WITH SOLAR SYSTEM ABUNDANCES*

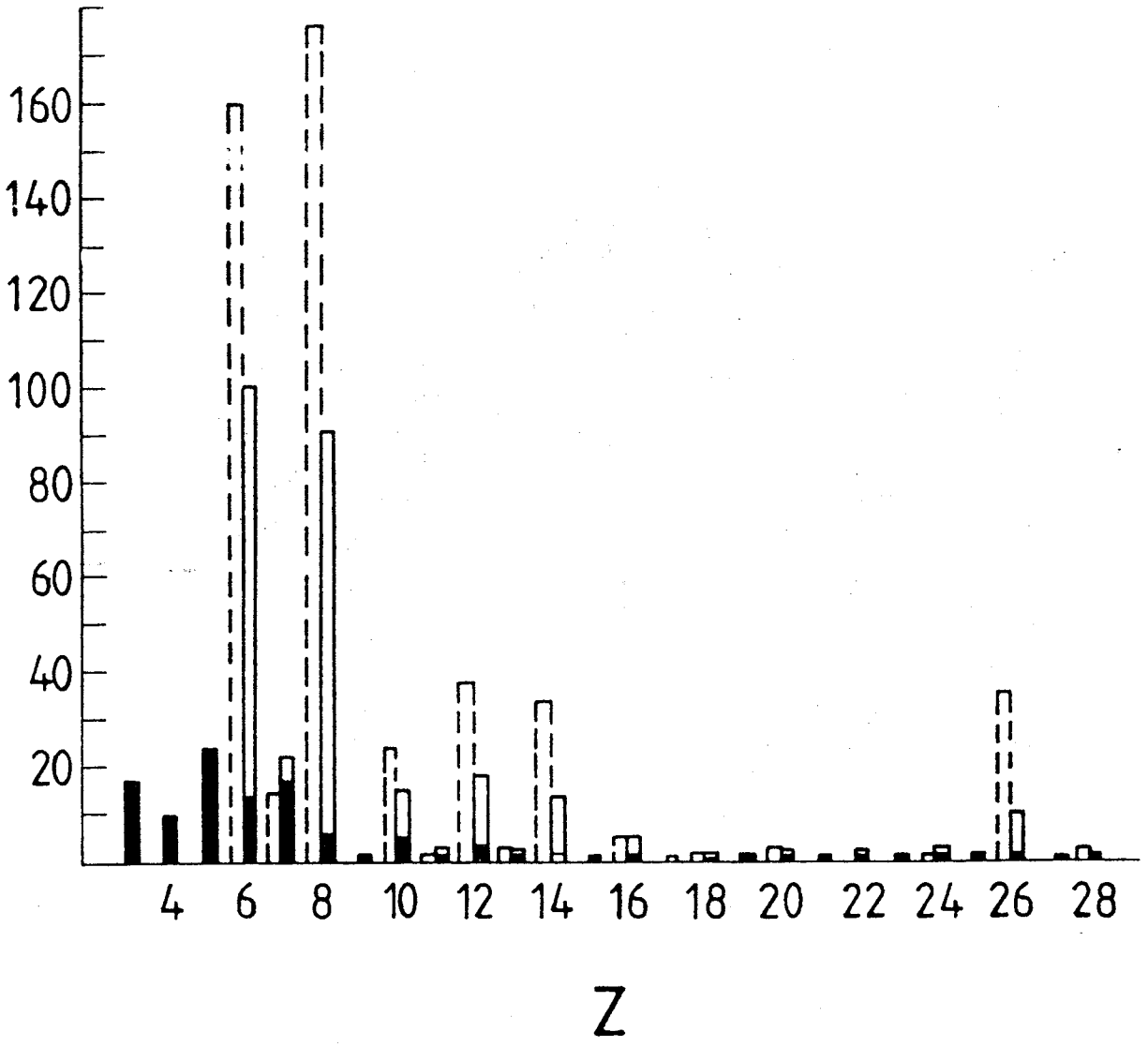


Dashed bars show source composition. Adjacent bars show arriving composition, the filled portion being nuclei produced by fragmentation and the open portion surviving primordial nuclei.

*FIGURE 3.7 - COSMIC RAY FRAGMENTATION*

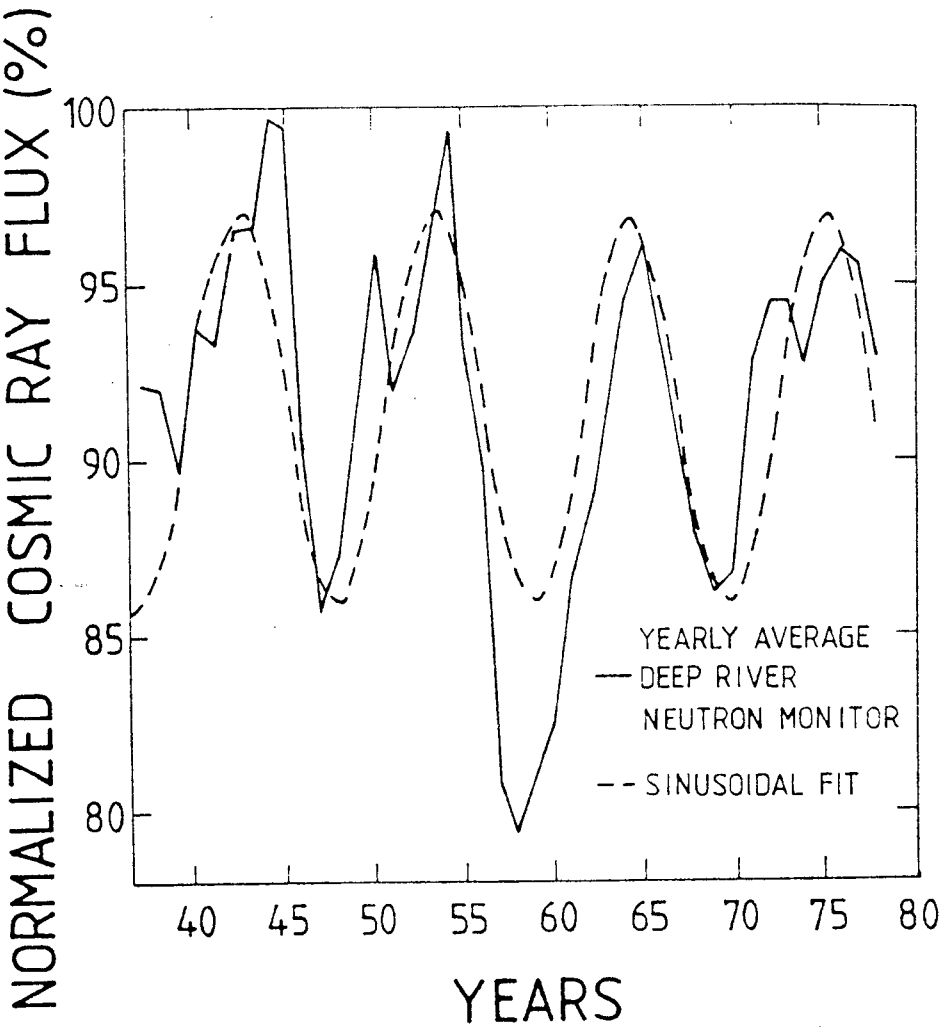


*FIGURE 3.8 - THE 11-YEAR SOLAR CYCLE AS MEASURED BY THE GROUND - LEVEL COSMIC-RAY INTENSITY AT THE DEEP RIVER NEUTRON MONITOR (ONTARIO, CANADA)*

### 3.4.4. Geomagnetic shielding

For cosmic rays to reach a spacecraft in earth orbit or the Earth's surface, they must penetrate the Earth's magnetic field. Since they are moving charged particles, they will tend to be deflected by the magnetic field. However, this tendency is opposed by the energy of the particles as they move at high velocity towards the Earth. A particle's penetrating ability is determined by its momentum divided by its charge and this quotient is referred to as its "magnetic rigidity".

So, for each point within the Earth's magnetic field, there is a minimum magnetic rigidity which a cosmic ray requires to reach that point. Particles below the minimum will be deflected and this minimum is called the geomagnetic cut-off value. As mentioned earlier, geomagnetic disturbances may affect the cut-off, lowering it. The cut-off value falls to zero at the edges of the magnetosphere and at the Earth's magnetic poles. Since the cosmic ray flux is highest at low energies, a satellite in earth orbit will be protected to some extent from cosmic rays by the magnetic field. The degree of protection will depend on the altitude and orientation of the orbit (Adams et al, 1983 and Adams, 1986). Geostationary orbits are afforded virtually no geomagnetic shielding against cosmic rays and polar orbits are also significantly exposed.

### 3.4.5. Other sources of cosmic rays

Adams (1981) referred to two other sources of energetic charged particles in the interplanetary medium. "Co-rotating events" give rise to infrequent modest increases in particle flux in the energy range up to 20 MeV. The particles are thought to be ejected from the high-energy tail of the solar wind and the streams are correlated with phenomena co-rotating with the Sun.

The "anomalous cosmic ray component" makes a more significant contribution but, near the Earth, appears infrequently at each solar minimum or at alternate ones. The anomalous spectra are observed for helium, nitrogen and oxygen and it is thought that the particles involved are singly charged. Their origin could be clouds of neutral interstellar gas entering the solar system. They become ionised as they approach the Sun and are then accelerated in collisions between fast and slow moving streams of solar wind. The energies of the nuclei are mainly in the range 1 to 30 MeV. An important point is that, if the anomalous component is only singly charged, the particles will penetrate deeper into the magnetosphere than cosmic rays of similar mass and energy.

## 3.5. LOW-ENERGY PARTICLES AND PLASMA

At the other end of the energy spectrum, protons and electrons in the energy range up to about 100 KeV are encountered throughout

the space environment. Within the trapped radiation belts, these particles merely represent the low-energy extremes of the trapped electron and proton populations.

Since these particles will be stopped effectively by minute thicknesses of material, only the most exposed surfaces are expected to be vulnerable. Thermal-control surfaces of spacecraft will be affected. These particles can penetrate sensors on some astrophysics satellites and produce a "background" signal.

Of course, the plasma environment at geostationary altitudes is well known for its ability to induce high levels of electrostatic charging on spacecraft. Energetic particles are also known to cause charging of internal spacecraft dielectrics such as those found on cabling, etc.

## 3.6. OTHER PLANETS

This subject is of special importance at the present time when long-term missions to remote parts of the solar system are under way or being planned. The giant planets have trapped radiation belts similar to, but more intense than, Earth's. Measurements of Jupiter's environment have been made by the Pioneer 10 and Voyager spacecraft and, more recently, by Ulysses, and a great deal of work has been carried out to prepare spacecraft electronics for survival in that environment. There are reports suggesting that Jupiter's electrons are occasionally transported to the Earth's magnetosphere (Baker et al, 1986). Saturn is also known to have an energetic radiation environment.

## 3.7. SECONDARY RADIATION

When real spacecraft are considered, the natural radiation environment is complicated by the secondary effect of "Bremsstrahlung" (brake-radiation) X-rays. This type of radiation is caused when electrons are slowed down in any way, e.g. by their interaction with the spacecraft material. Megavolt Bremsstrahlung will penetrate about one centimetre of aluminium with only 10% loss of intensity. It can sometimes therefore be considered as having an irreducible effect on unmanned spacecraft which are rarely constructed of aluminium thicker than 3 to 8 mm.

Secondary protons and neutrons are generated by high-energy protons in space. Radioactivity induced by high-energy nuclei in spacecraft is at a level too low to produce component degradation, but can interfere with instrument operation.

The products of proton-induced nuclear interactions can cause component upset (see below).

## 3.8. PREDICTION OF RADIATION LEVELS - ENVIRONMENTAL MODELS

### 3.8.1. General

The foregoing sections make it clear that, owing to the highly structured nature of the trapped radiation environment, the flux received at the surface of Earth-orbiting spacecraft varies considerably with orbital altitude and inclination. Figure 3.2 shows for example that a polar orbit will pass four times through the cusps of the outer zone even though an equatorial orbit at the same altitude may be well inside the inner zone. Other effects arise from geomagnetic anomalies. Figure 3.4 shows that low-altitude circular orbits will continually pass through the South Atlantic anomaly, giving rise to a highly variable flux exposure. Geostationary satellites, with a fixed geographic latitude, will vary in geomagnetic latitude depending on their longitude, because of the tilted field axis, and will thus experience different fluxes. Furthermore, as described earlier, the effect of the solar wind is to distort the Earth's field, and hence the radiation belts, into a highly asymmetric shape, so that a spacecraft - even if describing a circular equatorial orbit - will be subject to a diurnally (day-night) varying flux of particles. It will be clear also that time factors such as the solar activity cycle are influential.

In response to the obvious need for quantitative prediction of radiation levels likely to be encountered during space missions, models of trapped radiation environment have been constructed. These present data in graphical and numerical form and allow either manual calculation or computer handling. The models were derived from measurements by particle detector equipment aboard a large number of spacecraft. The standard models were produced by the National Space Science Data Center (NSSDC at NASA Goddard SFC).

Since the radiation environment is in a continual state of change, either rapid or slow, no published model is ever completely up-to-date. Successive versions reflected these changes together with improvements in particle measurement and data handling techniques and new data from scientific probes in orbit. However, the most recent models are based on satellite data acquired before 1971. The reader is referred to Holmes-Siedle et al. (1985), McCormack (1986), Gussenhoven et al. (1987) and Gussenhoven et al. (1991) for reports of comparisons between flight experience and model predictions.

It is useful to note various terms and conventions before describing the models in more detail:

(i) Particle fluxes, usually described as "omnidirectional", are often considered as isotropic from all directions. In fact, omnidirectional really means treating fluxes from all directions equally. It is a subtle difference, but the variation of omnidirectional flux along a field line can be used to derive the directional distribution at any point (Hess, 1968).

(ii) "Orbital integrations" are presented for various altitudes and inclinations. The fluxes quoted are averages around an orbit, thus allowing for the passage of an orbit through different radiation zones.

(iii) "Integral flux" is the total flux ($cm^{-2}\ s^{-1}$) at all energies above a quoted threshold energy. "Differential flux" is the rate of change of flux with energy at a specific energy ($cm^{-2}\ s^{-1}\ MeV^{-1}$).

(vi) Models are ascribed to particular epochs and versions relate specifically to either solar minimum or solar maximum conditions.

The latest NSSDC models are described below. They are distributed as hard copy, microfiche and in computer-readable form. The models are described by FORTRAN BLOCK DATA subprograms in the format originated by Kluge and Lenhart (1971). Here, the equatorial $\log_{10}$ fluxes at discrete energy (E) and L values are stored and the B variation described by tabulating at each (E, L) point the changes in $B/B_0$ required for constant $\log_{10}$ flux decreases. $B_0$ is the field strength at the geomagnetic equator where the field is a minimum. So, as normally distributed, these models provide integral omnidirectional fluxes as functions of E, L and $B/B_0$.

There are other features of the radiation environment which may be important in some situations such as flux anisotropy (Watts et al. 1989), diurnal (day-night) variations described above and short-term (e.g. magnetic storm) effects. The NSSDC documentation for earlier models (e.g. Teague and Vette, 1972, Singley and Vette, 1972) describe forms of those models which included pitch-angle distributions, local-time dependence and a statistical model. The condensed-format convention for the new models does not include these features (although pitch-angle distributions can be derived from the B variation as mentioned above).

McCormack (1986) reported on the importance of the choice of geomagnetic field epoch used when accessing the NSSDC

environment models. Before the fluxes are computed from the models, it is necessary to compute the geomagnetic B-L co-ordinates of the point of interest by using a geomagnetic field model. Problems arise from the fact that the geomagnetic field is varying slowly. As pointed out above, the environment data were acquired in the 1960s. Since then the field has decayed and shifted somewhat and predictions of further "secular" variations to the 1990s or beyond yield a significantly modified field. The data were obviously organised according to the 1960 field. Using updated or extrapolated field epochs implies that, because the field has shifted, corresponding field lines are closer to the Earth and the radiation belts have come down to lower altitude giving higher exposure in low-Earth orbit. The fact is that the radiation environment is not permanently frozen on a field line, but is the result of an equilibrium between continual creation and loss processes (Daly, 1989). The observed environment has in fact varied less in spatial terms than if it were tied so closely to the varying geomagnetic field. The initial recommendation of the NSSDC was that geomagnetic model epochs should not be extrapolated beyond the 60's in using these models. Lemaire et al. (1990) point out that no extrapolation should be performed.

### 3.8.2. Trapped electrons - AE8

AE8 is a model for the electron environment for energies of 40keV to 7MeV and L values of 1.2 to 11 $R_E$. It is available in two versions, AE8MAX and AE8MIN for solar maximum and solar minimum periods respectively. These models have only recently been documented (Vette, 1991). Figure 3.9 shows the radial variation of the model omnidirectional fluxes at the geomagnetic equator for three energy thresholds. The models replace previous models for inner-zone electrons and models for outer-zone electrons whose documentation is still of some relevance to the AE8 model (Teague and Vette, 1974 and Teague et al., 1976).

At low energy and equatorially, the AE8 model looks much like the previous models. At high energy in the outer zone, the fluxes are generally below those of its predecessor, the AEI7 model. The location along the field line of the atmospheric cutoff of fluxes has also been revised, leading again to a lowering of fluxes. Figure 3.10 shows a comparison of AE8 equatorial radial flux variations at E > 4MeV and those for the AEI7 models. Figure 3.11 shows a comparison between the flux variations along the field lines at E > 2MeV and L=3 and 5. An example of the electron spectrum derived from the AE8MAX model when an average is performed over a geostationary orbit (see Section 18, "Computer Methods") is given in Figure 3.12.

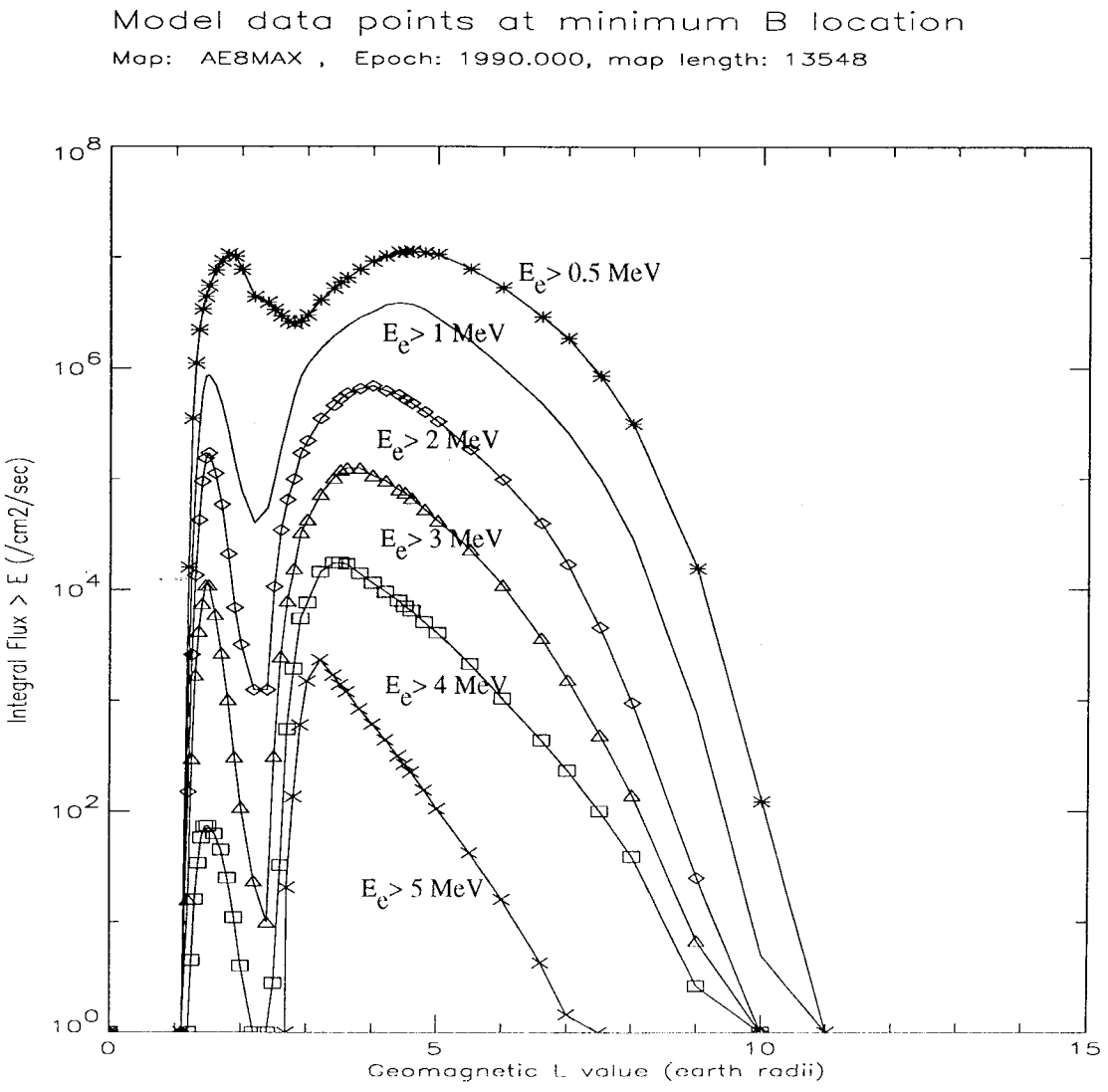


Radial variation of AE8 model omnidirectional fluxes at the geomagnetic equator for three energy thresholds.

*FIGURE 3.9 - RADIAL ELECTRON FLUX VARIATIONS*

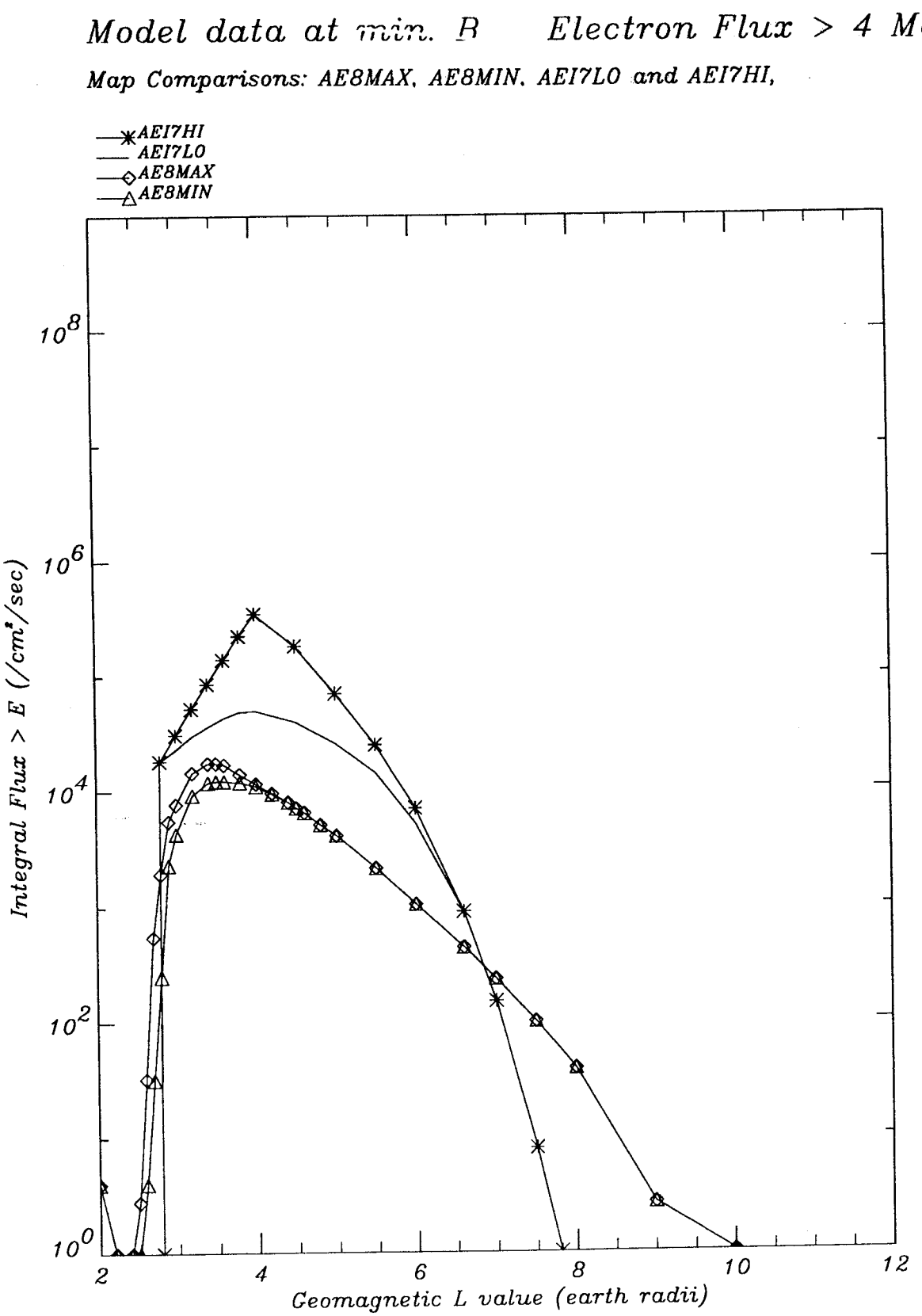


A comparison of equatorial radial variations of AE8 model omnidirectional fluxes at E > 4 MeV with those for the AEI7 models.

*FIGURE 3.10 - COMPARISON OF ELECTRON MODELS AE8 AND AEI7*

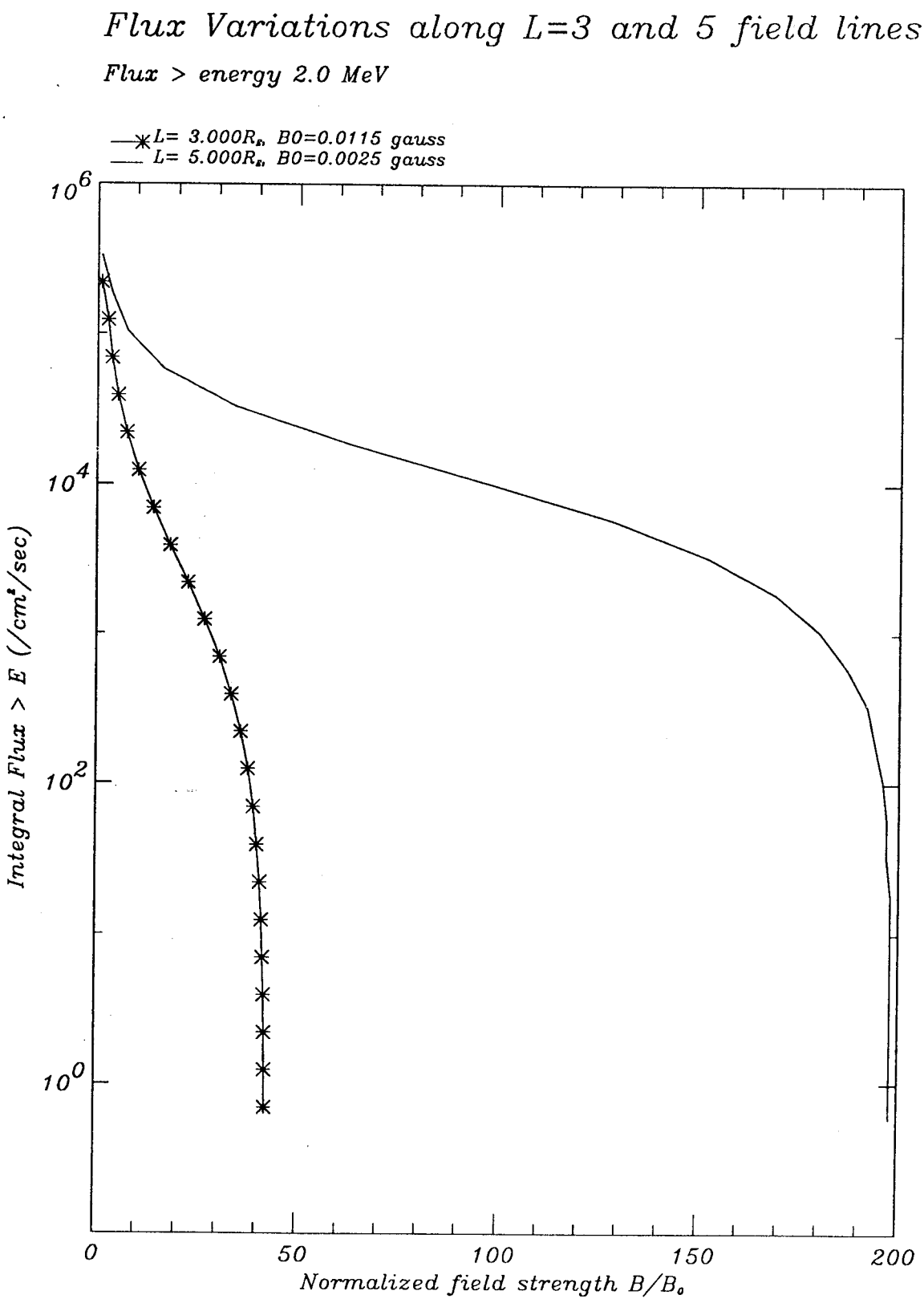


A comparison between the electron flux variations along the field lines at E > 2 MeV and L=3 and 5.

*FIGURE 3.11 - AE8 FLUX VS. B VARIATIONS*

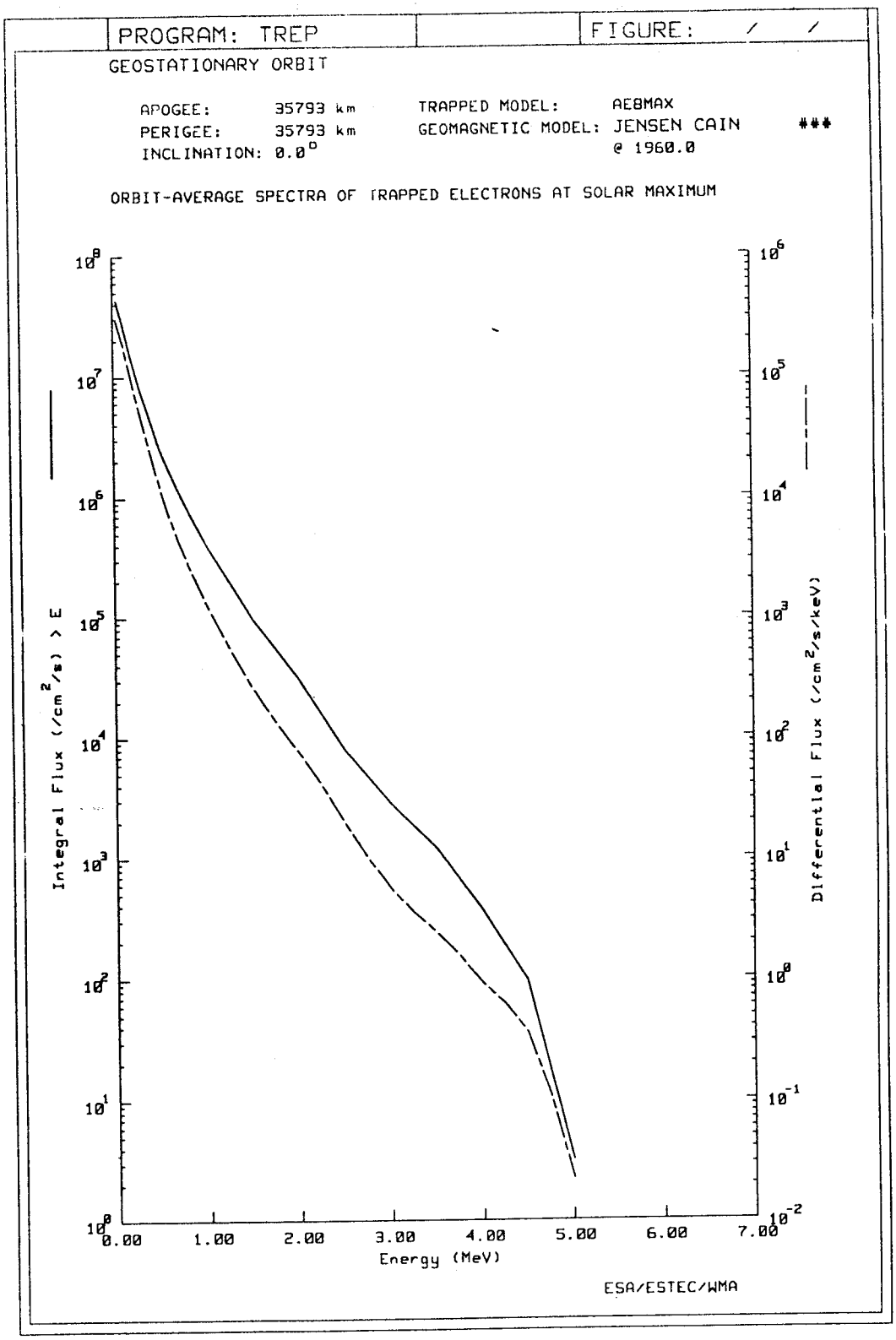


Example of electron spectrum derived from the AE8MAX model when an average is performed over a geostationary orbit.

*FIGURE 3.12 - EXAMPLE ELECTRON SPECTRUM*

### 3.8.3. Trapped protons - AP8

The AP8 model (Sawyer and Vette, 1976) is the latest model of the trapped proton environment for energies of 100 keV to 400 MeV and L values of 1.15 to 6.6 $R_E$. Again, it contains solar maximum and solar minimum versions, AP8MAX and AP8MIN respectively, which are distributed as FORTRAN BLOCK DATA subprograms in the format of Kluge and Lenhart, providing average omnidirectional fluxes as functions of E, L and B.

Figure 3.13 shows plots of AP8 equatorial radial flux variations at a number of energy thresholds. Figure 3.14 shows the flux variations along the field lines at E > 20 MeV and the L=1.5, 2 and 3. An example of the proton spectrum derived from the AP8MIN model when an average is performed over a circular low Earth orbit (500 km, 28°) is given in Figure 3.15.

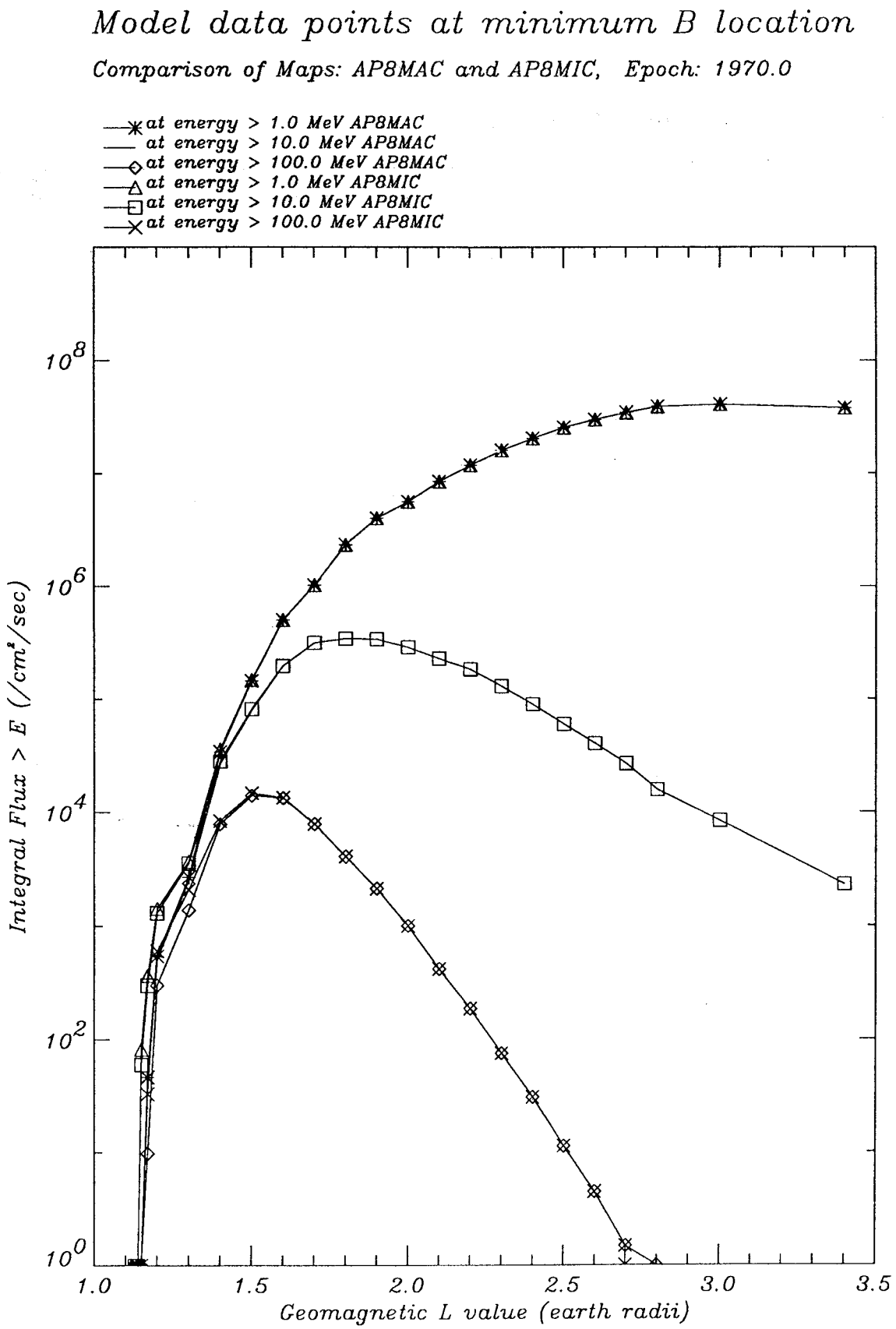


Plots of AP8 model equatorial flux radial variations at a number of energy thresholds.

*FIGURE 3.13 - RADIAL PROTON FLUX VARIATIONS*

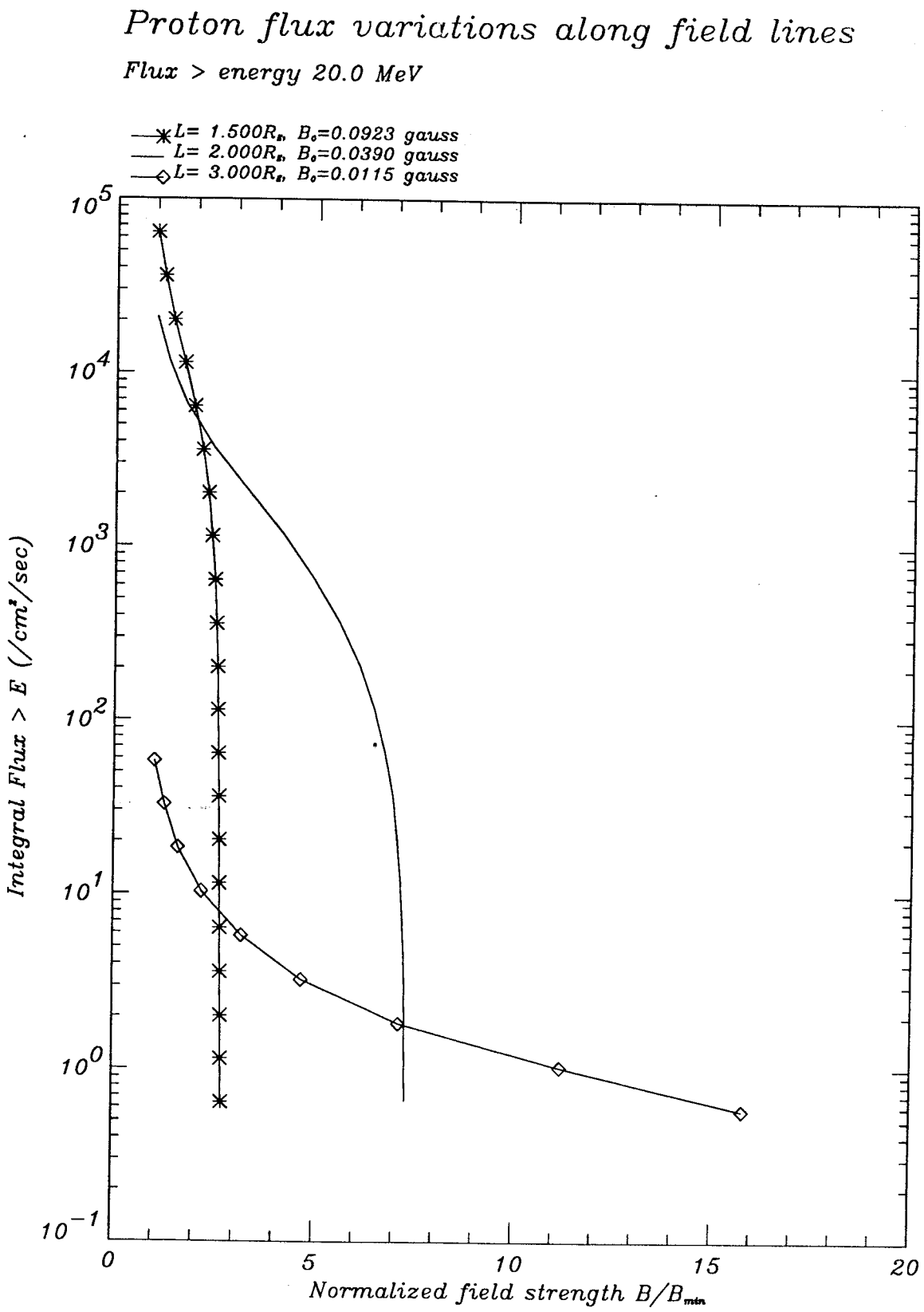


The figure shows the proton flux variations along the field lines at E > 20 MeV and L=1.5, 2 and 3.

*FIGURE 3.14 - PROTON FLUX VARIATIONS WITH B.*

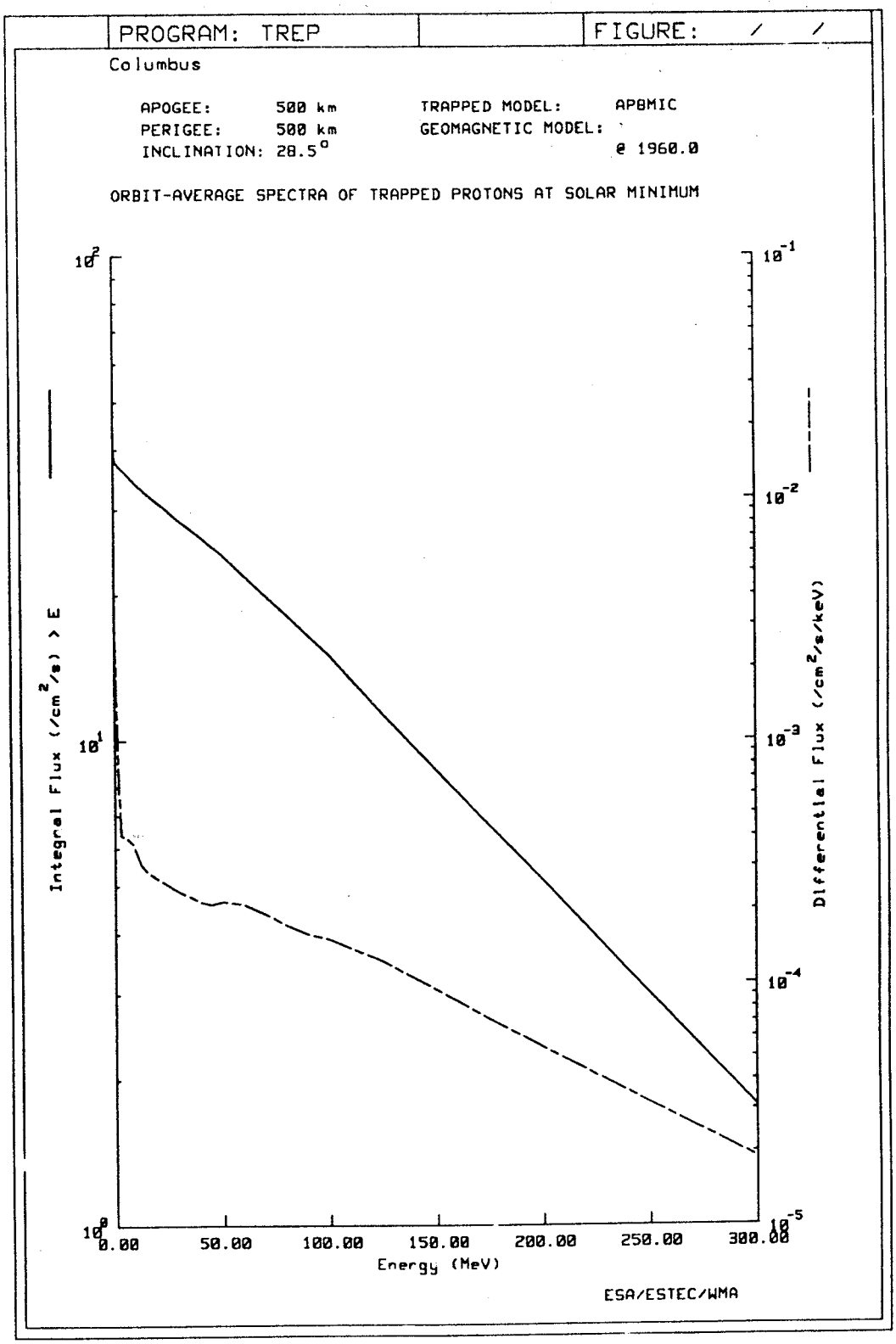


Example of Proton Spectrum derived from the AP8MIN model when an average is performed over a circular low earth orbit (500 km, 28°).

*FIGURE 3.15 - EXAMPLE OF PROTON SPECTRUM*

### 3.8.4. Solar flare protons

Predicting solar-proton fluxes and constructing a model on which to base calculations is an entirely different matter from that associated with trapped radiation. The problem has been tackled by NASA and predictions for solar cycle 21 (1974 - 1985) have resulted from the work of King (1984) and Stassinopoulos and King (1984). King's work was essentially based on one solar cycle's worth of data. Recently, Feynman et al. (1990) evaluated three cycles and produced a new statistical model and the models were compared with each other and the event record by Tranquille and Daly (1992).

For prediction purposes, it has been found most reasonable to regard the solar cycle as consisting of seven active years, in which significant solar-proton flux may be expected, and four quiet years during which only minor events occur.

The history of recent cycles is shown in Figure 3.16 from Tranquille and Daly (1992), while Figure 3.17 gives the integral flux predicted by the King model on the above simple model for three energy thresholds over the seven active years. The actual annual fluence for cycle 20 at the 10 MeV threshold is also shown. A flux versus energy spectrum based upon this model is included in Figure 3.18. The difficulty in making such a prediction is illustrated by the fact that in the very active year of 1972 almost all this year's fluence was received during one August week; in fact, the contribution from this one week represents 67% of the total fluence for the entire seven years.

Flares are assessed on a statistical basis. The King model is based on the observation of one anomalously large (AL) flare of the August 1972 type in a 7 year period. A worst-case assessment is normally made, yielding a number of flare events with a high probability (90% or even 95%) that the number of flares will not be exceeded. This modified Poisson statistic is due to Burrell and is described by King (1974). The table below shows the probability of occurrence of flares in a seven-year period given that one was observed in a previous seven-year period.

| Number of Events n | Probability of n |
|---|---|
| 0 | 25% |
| 1 | 25% |
| 2 | 19% |
| 3 | 12% –> 81% confidence of no more |
| 4 | 8% –> 89% confidence of no more |
| 5 | 5% –> 94% confidence of no more |
| 6 | 3% –> 97% confidence of no more |

In the model of Feynman et al., no distinction is made between ordinary and anomalously large events since all are found to lie on a log-normal fluence distribution, as shown in Figure 3.19. The Feynman model is now recommended as the standard. A detailed comparison between the models of King and Feynman et al. was performed by Tranquille and Daly (1992). This showed, for example, that the worst one-year period in the solar event record corresponds to a confidence level in the Feynman et al. model for more than 96%, indicating that high confidence levels are not unduly pessimistic. They also make comparisons between the models and more recent data. Figure 3.20, from their work, shows comparisons between King and Feynman et al. model spectra for various periods.

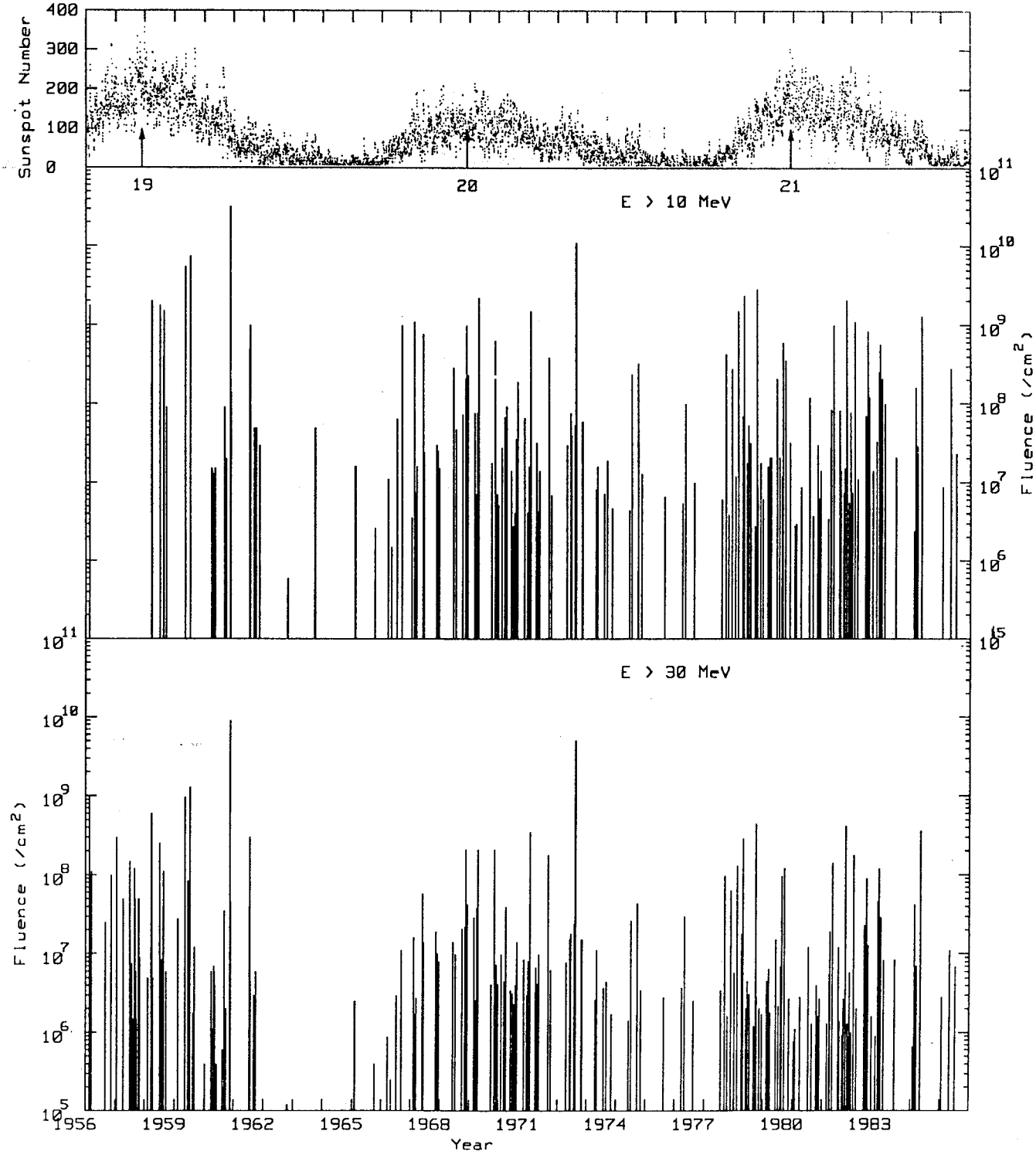


Solar activity cycles 19, 20 and 21. This shows the periodicity of sunspot maxima and minima and the way particle events are linked to this periodicity. Event-integrated proton fluences are shown for two energy thresholds (Tranquille and Daly 1992).

*FIGURE 3.16 - SOLAR ACTIVITY OVER 3 SOLAR CYCLES*

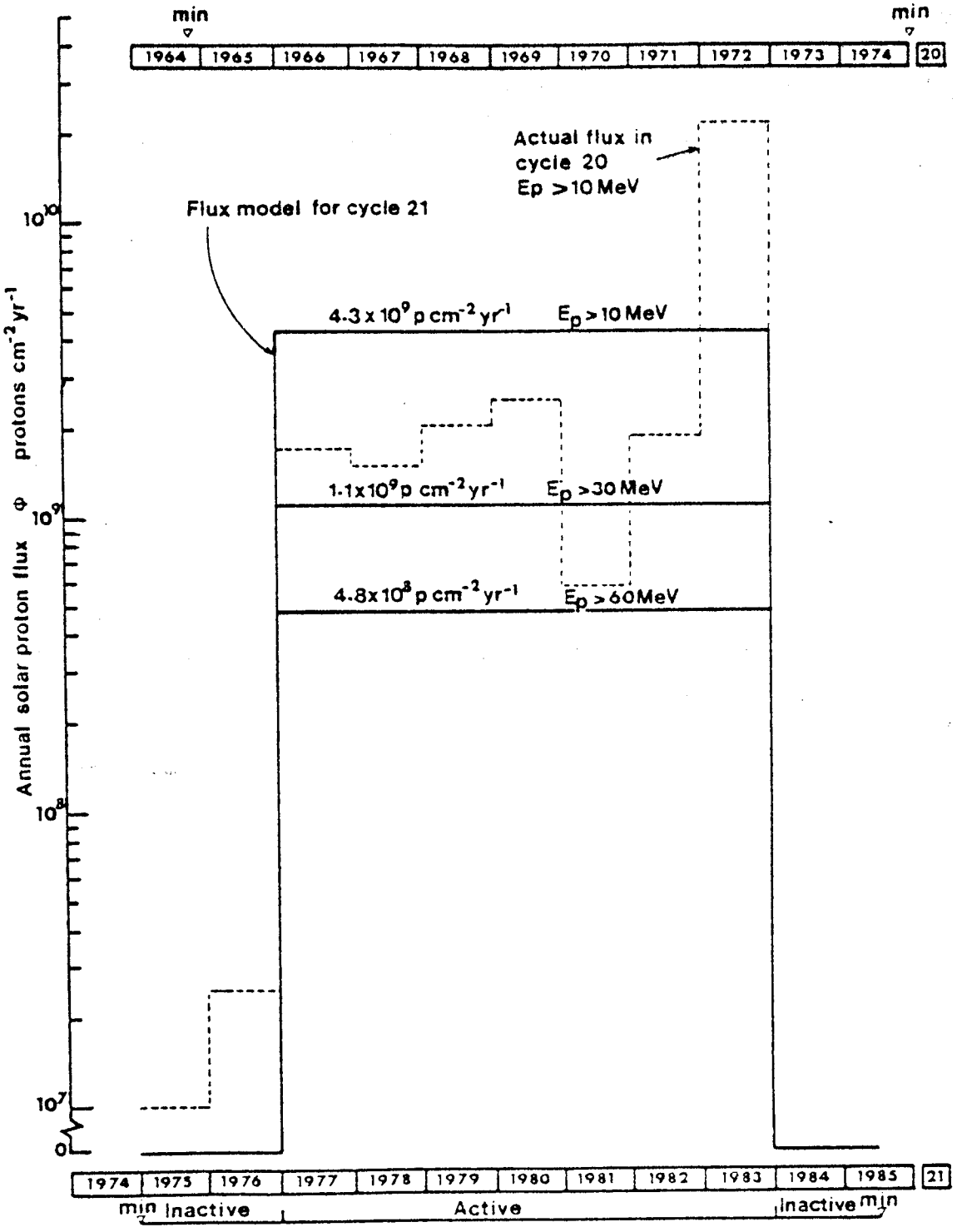


Predicted model for solar-flare proton integral flux in free space at Earth's orbit, for solar cycle 21.

*FIGURE 3.17 - SOLAR PROTON MODEL*

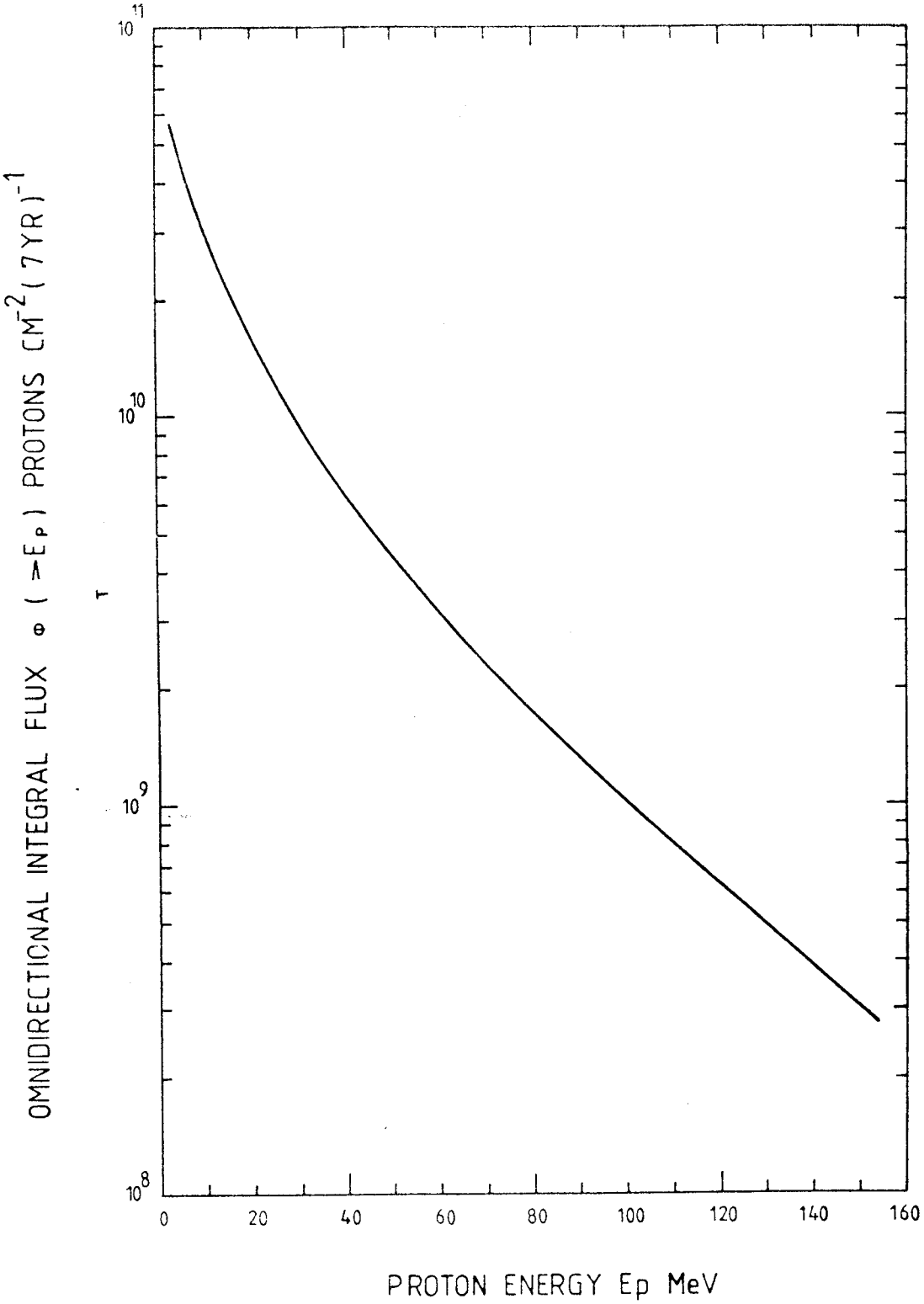


Integral flux spectrum derived from the model for solar cycle 21. Seven active years.

*FIGURE 3.18 - SOLAR PROTON SPECTRUM*

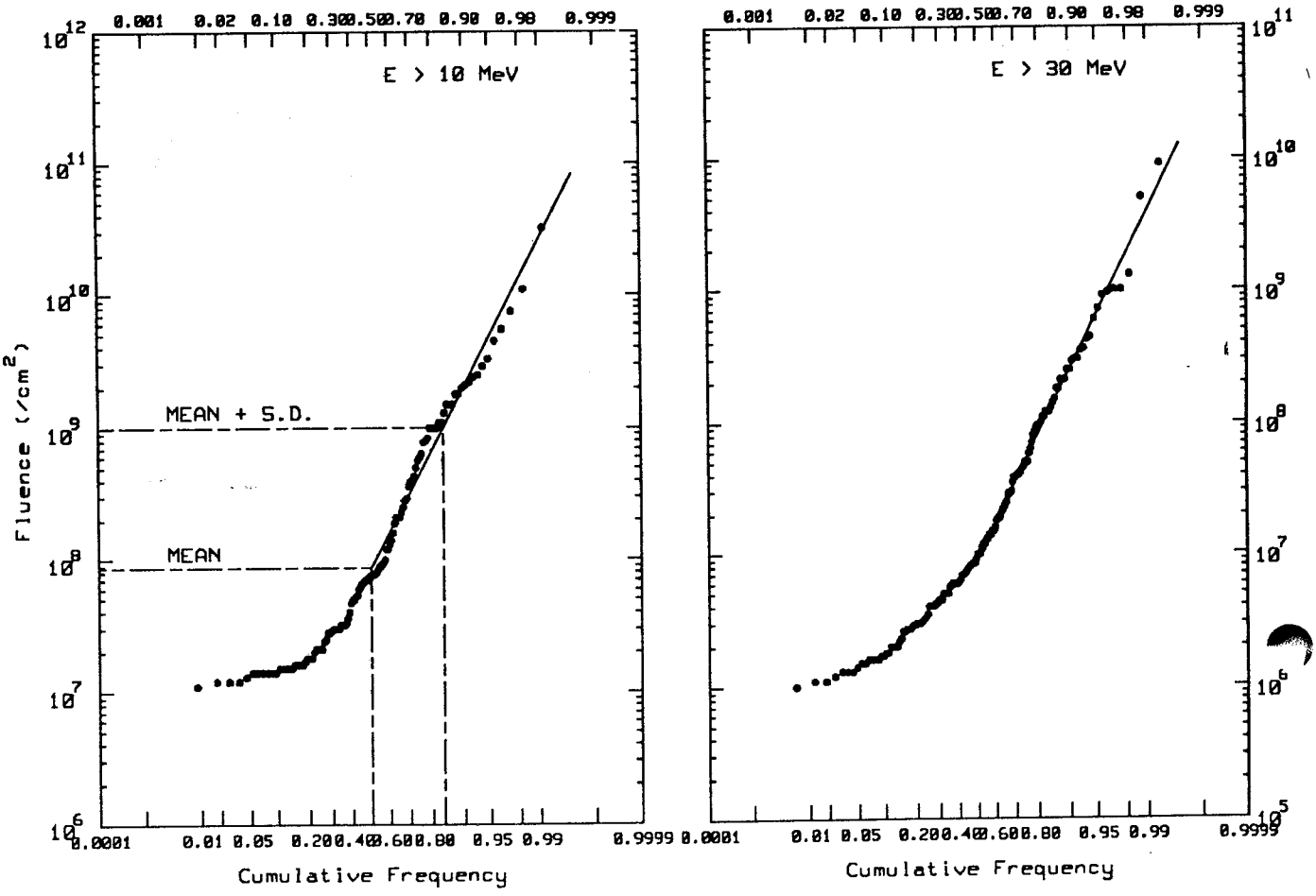


The Cumulative Event Fluence Distribution use for the statistical event model of Feynman et al. This shows that even large events follow a log-normal distribution. (From Tranquille and Daly, 1992).

*FIGURE 3.19 - THE CUMULATIVE EVENT FLUENCE DISTRIBUTION*

The models are based upon conditions of free space (outside the Earth's magnetic field) at the Earth's orbital distance from the sun. However, we have already mentioned in Section 3.4.4. that geomagnetic shielding keeps some particles from reaching certain locations. Stassinopoulos and King also consider the likelihood of the solar protons penetrating the Earth's field. It is assumed that protons in the energy range 10-100 MeV can be expected to penetrate to magnetic shell L = 5 approximately. Thus, a satellite in geostationary orbit may be considered to be completely exposed, while one in an equatorial orbit at 18 530 km altitude L = 3.9) is to be considered to be completely shielded by the Earth's field. In polar or highly inclined orbits, of course, spacecraft may pass back and forth between regions of high L (high exposure) and low L (effective shielding). "Percentage exposure" maps, relating solar proton exposure to orbital altitude and inclination, are provided by Stassinopoulos and King (1984).

The direction of arrival at a point in the Earth's field also plays a role in geomagnetic shielding. It can be shown (e.g. Daly, 1988) that cosmic rays penetrate the geomagnetic field more easily from the west than from the east. Computing the geomagnetic cut-off for vertically arriving protons shows that the Stassinopoulos and King model corresponds to excluding protons of E < 200 MeV from arriving vertically al L < 5 in a quiet magnetosphere. Figure 3.20 (from Daly, 1988) however, shows that protons of lower energy can penetrate below L=5 with other arrival directions, especially in a disturbed magnetosphere where the geomagnetic shielding is weakened. For westward arrival at the L=5 geomagnetic equator in a disturbed magnetosphere, the energy cut-off could be as low as 30 MeV. An arrival-direction-dependent model for flare-proton cut-offs throughout B, L space can be used by the ESA UNIRAD system (see Section 18 "Computer methods"). Recently, Gussenhoven and Muller (1992) have reported that during the March 1991 solar-proton event, the CRRES satellite observed abnormally deep penetration of solar protons into the inner magnetosphere.

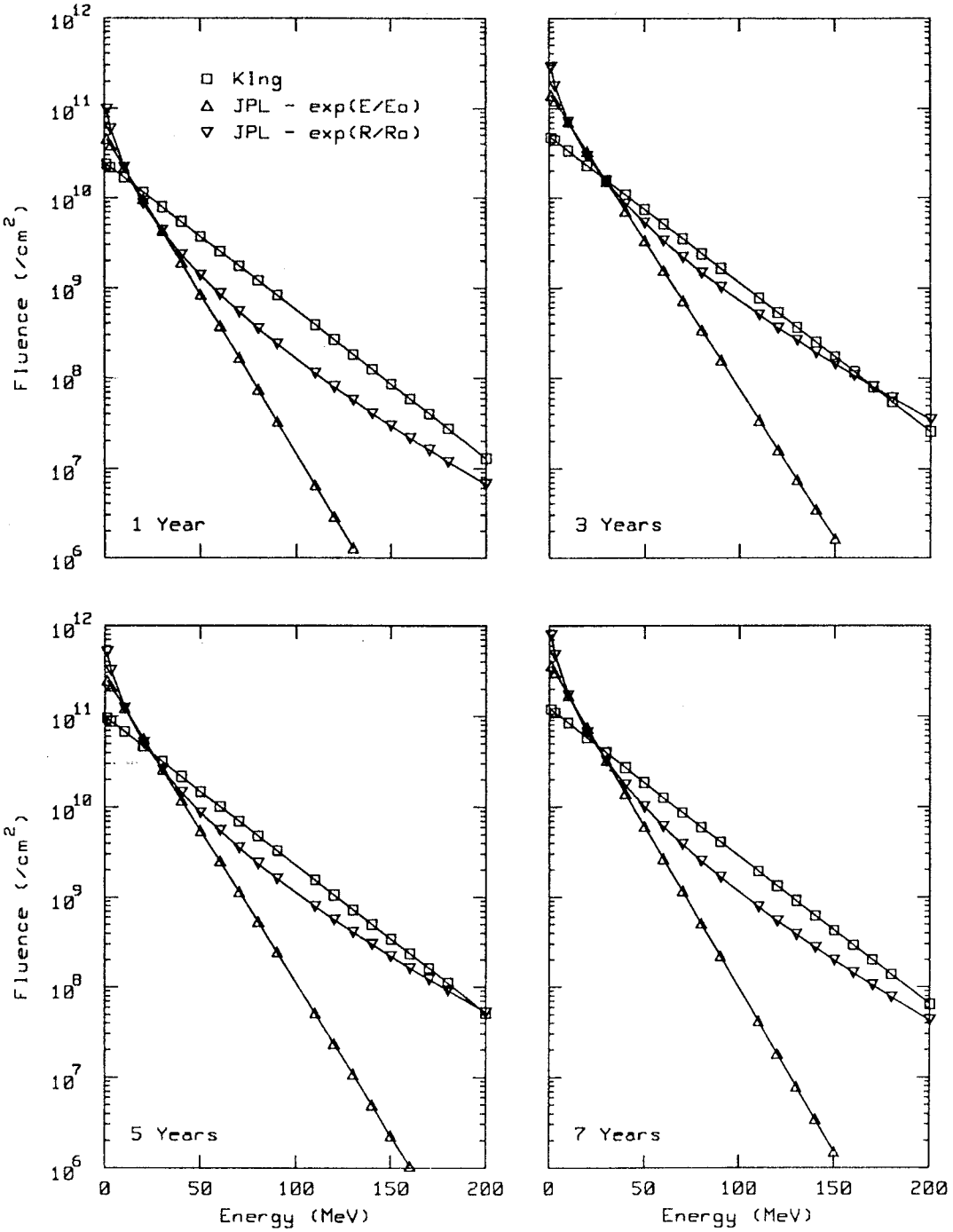


*FIGURE 3.20 - COMPARISONS BETWEEN SOLAR PROTON SPECTRA FROM MODELS OF KING AND OF FEYNMAN ET AL.*

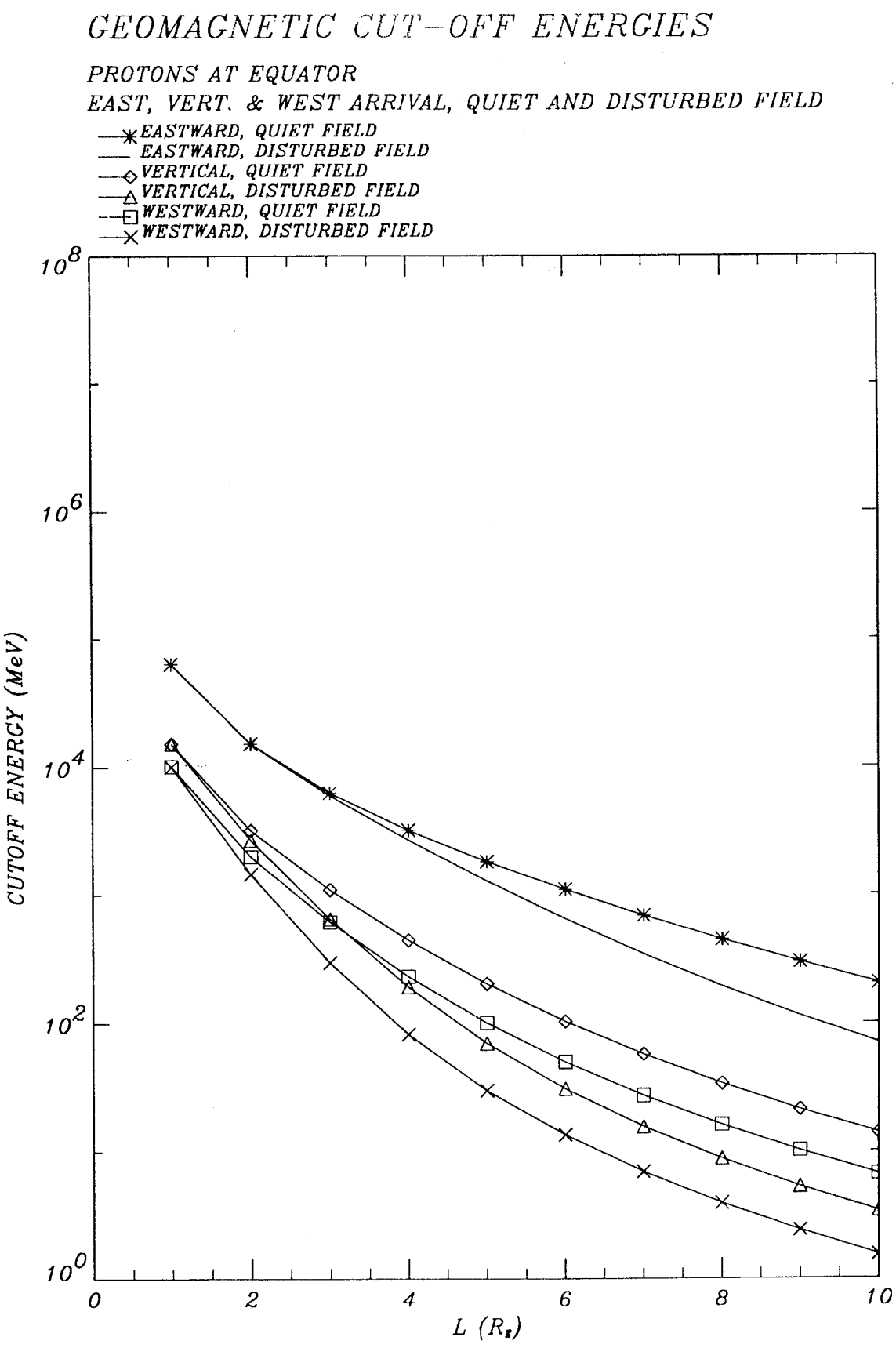


FIGURE 3.21- PROTON CUT-OFF ENERGIES

### 3.8.5. Environments for specific orbits

To estimate radiation levels likely to be encountered in specific missions, data from the appropriate environment models must be processed in such a way as to provide orbit-integrated particle flux spectra for specific orbital parameters. This is particularly relevant to other than simple circular orbits. Computer programs for the provision of orbital environments for a range of missions are used widely throughout the US and Europe. Software for the purpose is readily available (see Section 18 "Computer Methods").

### 3.8.6. Conclusions

The radiation environment models described represent the best estimates upon which predictions of exposure may be made. Models are undergoing continual re-appraisal and totally new models will be produced as a result of the high-quality data acquired by the CRRES mission. Initial results indicate important shortcomings in the models. However, it may be some time before new models are available.

A useful comparison between fluxes of the various types of natural radiation is made in Figure 3.21.

Successive sections of this document will discuss the effect of this radiation upon the performance of spacecraft components and describe the methods used to convert the environment data into estimates of radiation dose received by the components within the spacecraft structure.

### 3.8.7. Recommendations

It is recommended that:

- AE8 and AP8 be used as models for the trapped radiation environment, accessed using the Jensen and Cain model geomagnetic field with epoch 1960 for the solar minimum versions and GSFC 1966 with extrapolation to 1970 for solar maximum;
- the solar proton model of Feynman et al (1990) be used as the model for solar protons;
- the CREME models be used for heavy ions.

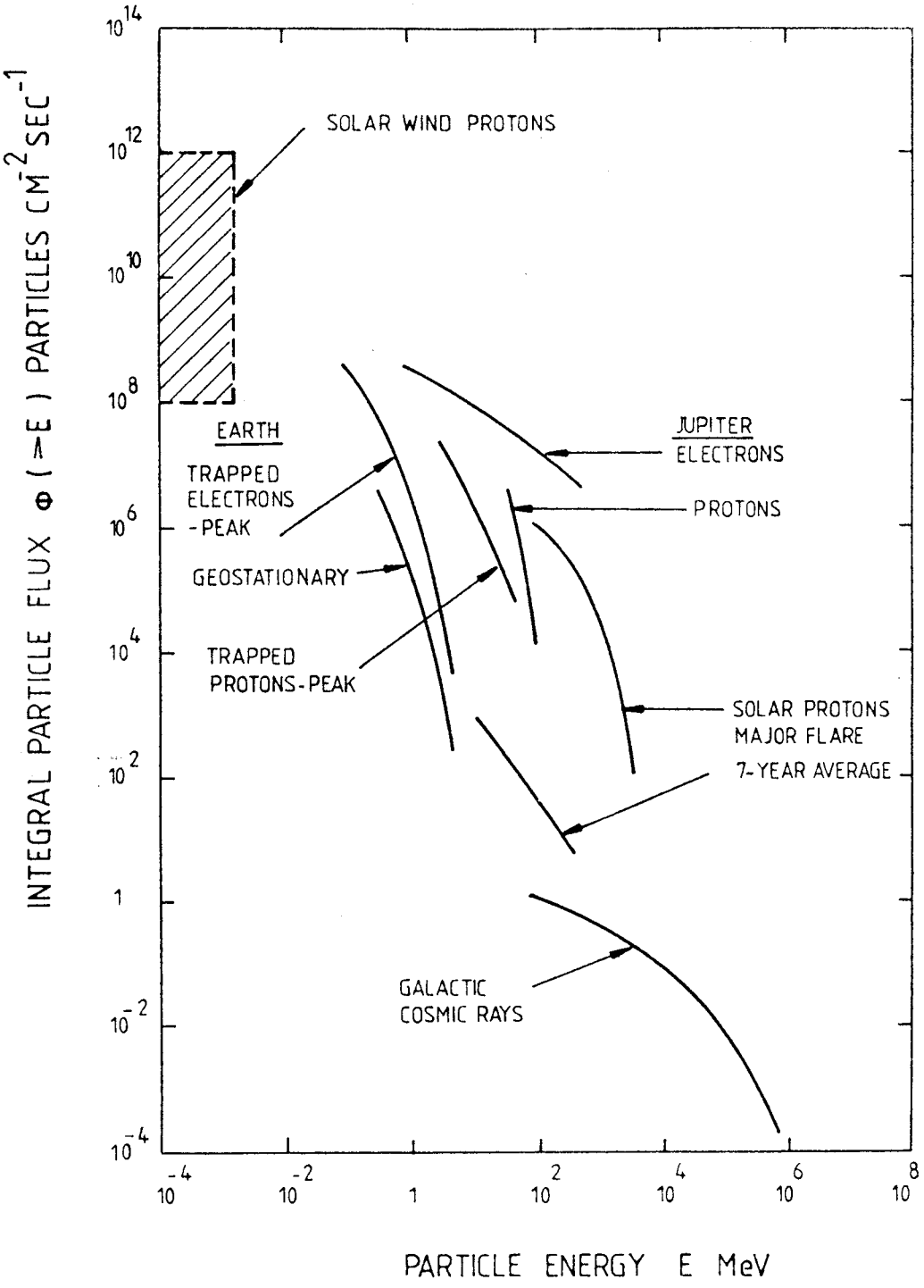


Integral spectra for the various components of the Earth's natural radiation environment. Jovian fluxes are shown for comparison.

*FIGURE 3.22 - SUMMARY OF RADIATION SPECTRA*

REFERENCES

Adams J.H., Letaw J.F. and Smart D.F., "Cosmic Ray Effects on Microelectronics Part I: The Near-Earth Particle Environment" NRL Memorandum Report 4506 1981.

Adams J.H., Letaw J.F. and Smart D.F., "Cosmic Ray Effects on Microelectronics Part II: The Geomagnetic Cutoff Effects", NRL Memorandum Report 5099 1983.

Adams J.H., "Cosmic Ray Effects on Microelectronics Part IV", NRL Memorandum Report 5901 1986.

Chenette D.L. and Dietrich W.F., "The Solar Flare Heavy Ion Environment for Single-Event"
Upsets: A Summary of Observations Over the Last Solar Cycle, 1973-1983", IEEE Trans. Nucl. Sci. NS-31, p. 1217, December 1984.

Daly E.J., "Models of the Earth's Radiation Environment", Estec Working Paper, 1987.

Daly E.J., "The Evaluation of Space Radiation Environments for ESA Projects", ESA Journal 12, 229 (1988).

Daly E.J., "Effects of Geomagnetic Field Evolution on Predictions of the Radiation Environment at Low Altitudes", ESTEC Working Paper 1531, January 1989.

Feynman J., Armstrong T.P., Dao-Gibner L. and Silverman S., "New Interplanetary Proton Fluence Model", J. Spacecraft and Rockets 27, 403,1990.

Goswami J.N., McGuire R.E., Reedy R.C., Lal D. and Jha R., "Solar Flare Protons and Alpha Particles During the Last Three Solar Cycles", J. Geophys. Res. 93, 7195 (1988).

Gussenhoven M.S., Mullen E.G., Filz R.C., Brautigam D.H. and Hanser F.A., "New Low-Altitude Dose Measurements", IEEE Trans. Nucl. Sci. NS-34, 676 (1987).

Gussenhoven M.S., Mullen E.G., Brautigam D.H., Holeman E., Jordan C., Hanser F. and Dichter B., "Preliminary Comparison of Dose Measurements on CRRES to NASA Model Predictions", IEEE Trans. Nucl. Sci. NS-38, 1655 (1991).

Gussenhoven M.S. and Mullen E.G., "Solar Particle Events as Seen on CRRES", Cospar paper F2.5-M.1.02, World Space Congress, Washington DC, September 1992.

Henley M.W., "Shielding Distribution for Anisotropic Radiation in Low Earth Orbit", J. Spacecraft and Rockets 23, p108, Jan 1986.

Hess W.N., "The Radiation Belt and the Magnetosphere", Blaisdell Publ. Co. (1968).

Holmes-Siedle A., Adams L., Marsden S. and Pauly B., "Calibration and Flight Testing of a Low-Field pMOS Dosimeter", IEEE Trans. Nucl. Sci. NS-32, p4425, December 1985.

King J.H., "Solar Proton Fluences for 1977-1983 Space Missions", J. Spacecraft and Rockets 11, p401, 1974.

Kluge G. and Lenhart K.G., "A Unified Computing Procedure for Trapped Radiation Models", ESRO/ESOC Internal Note 78, March 1971.

Konradi A., Hardy A.C. and Atwell W., "Radiation Environment Models and the Atmospheric Cut-off", J. Spacecraft 24, 284 (1987).

Lemaire J., Daly E.J., Vette J.I., McIlwain C.E. and McKenna-Lawlor S., "Secular Variations in the Geomagnetic Field and Calculations of Future Low Altitude Radiation Environments", Proc. ESA Space Environment Analysis Workshop, October 1990, ESA-WPP-23, in press. (Also Lemaire J. et al., ESA CR(P)-3126, September 1990.

Lyons L.R. and Williams D.J., "Quantative Aspects of Magnetospheric Physics", D. Reidel, Dordrecht, Holland, 1984.

McCormack P.D., "Radiation Dose and Shielding for the Space Station", paper IAF/IAA-86-380, 37th Congress of IAF, Innsbruck, Austria, October 1986.

McGuire R.E., Goswami J.N., Jha R., Lal D., Reedy R.C., "Solar Flare Particle Fluences During Solar Cycles 19, 20 and 21", 18th Int. Cosmic Ray Conference, Vol. 4, p66, Bangalore, India, 1983.

McIlwain C.E., "Coordinates for Mapping the Distribution of Magnetically Trapped Particles", J. Geophys. Res., 66, 3681, 1961.

Pruett R.G., "Comparison of DMSP and NTS-2 Dosimeter Measurements with Predictions", J. Spacecraft and Rockets 17, p270, 1980.

Teague M.J. and Vette J.I., "The Inner Zone Electron Model AE-5", NSSDC 72-10, November 1972.

Teague M.J. and Vette J.I., "A Model for the Trapped Electron Population for Solar Minimum", NSSDC 74-03, April 1974.

Teague M.J., Chan K.W. and Vette J.I., "AE 6: A Model Environment for Solar Maximum, NSSDC 76-04, May 1976.

Tranquille C. and Daly E.J., "An Evaluation of Solar Proton Event Models for ESA Missions", ESA Journal 16, 3, 275 (1992).

Tsao C.H., Silberberg R., Adams J.H. and Letars J.R., "Cosmic Rays Effects on Microelectronics, Part III": Propagations of Cosmic Rays in the Atmosphere, NRL Memorandum Report.

Sawyer D.M. and Vette J.I., "AP-8 Trapped Proton Environment for Solar Maximum and Solar Minimum",. NSSDC 76-06, December 1976.

Schultz M., "Earth's Radiation Belts", Review of Geopys. and Space Sci. 20, no.3, pp 613-621, August 1982.

Singley W. and Vette J.I., "The AE4 Model of the Outer Radiation Zone Electron Environment", NSSDC 72-06, August 1972.

Singley W. and Vette J.I., "A Model Environment for Outer Zone Electrons", NSSDC 72-13, December 1972.

Stassinopoulos E.G. and King J.H., "Empirical Solar Proton Model for Orbiting Spacecraft Applications", IEEE Trans. Aerosp. and Electr. Systems AES-10, p442, 1984.

Stassinopoulos E.G., "World Maps of Constant B, L and Flux Contours", NASA SP-3054, 1970.

Vette J.I. "The AE8 Trapped Electron Model Environment", NSSDC Report 91-24, NASA/GSFC November 1991.

Watts J.W., Parnell T.A. and Heckman H.H., "Approximate Angular Distribution and Spectra for Geomagnetically Trapped Protons in Low-Earth Orbit" in: High Energy Radiation Background in Space, Rester A.C. and Trombka J.I. (eds.), AIP (1989).

Ziegler J.F. and W.A. Landford, "The Effect of Sea Level Cosmic Rays on Electronic Devices", J. Appl. Physics 52 (6) June 1981.